Scientia is the Baylor Undergraduate Research Journal of Science and Technology. First published in the spring of 2014, *Scientia* is a yearly publication produced by Baylor Undergraduate Research in Science and Technology (BURST) and supported by the Baylor College of Arts and Sciences.

BURST's mission is to increase awareness of undergraduate research on the Baylor campus, provide opportunities for undergraduates to optimize their research experiences, and educate undergraduates in the proper habits and techniques of research in scientific fields.

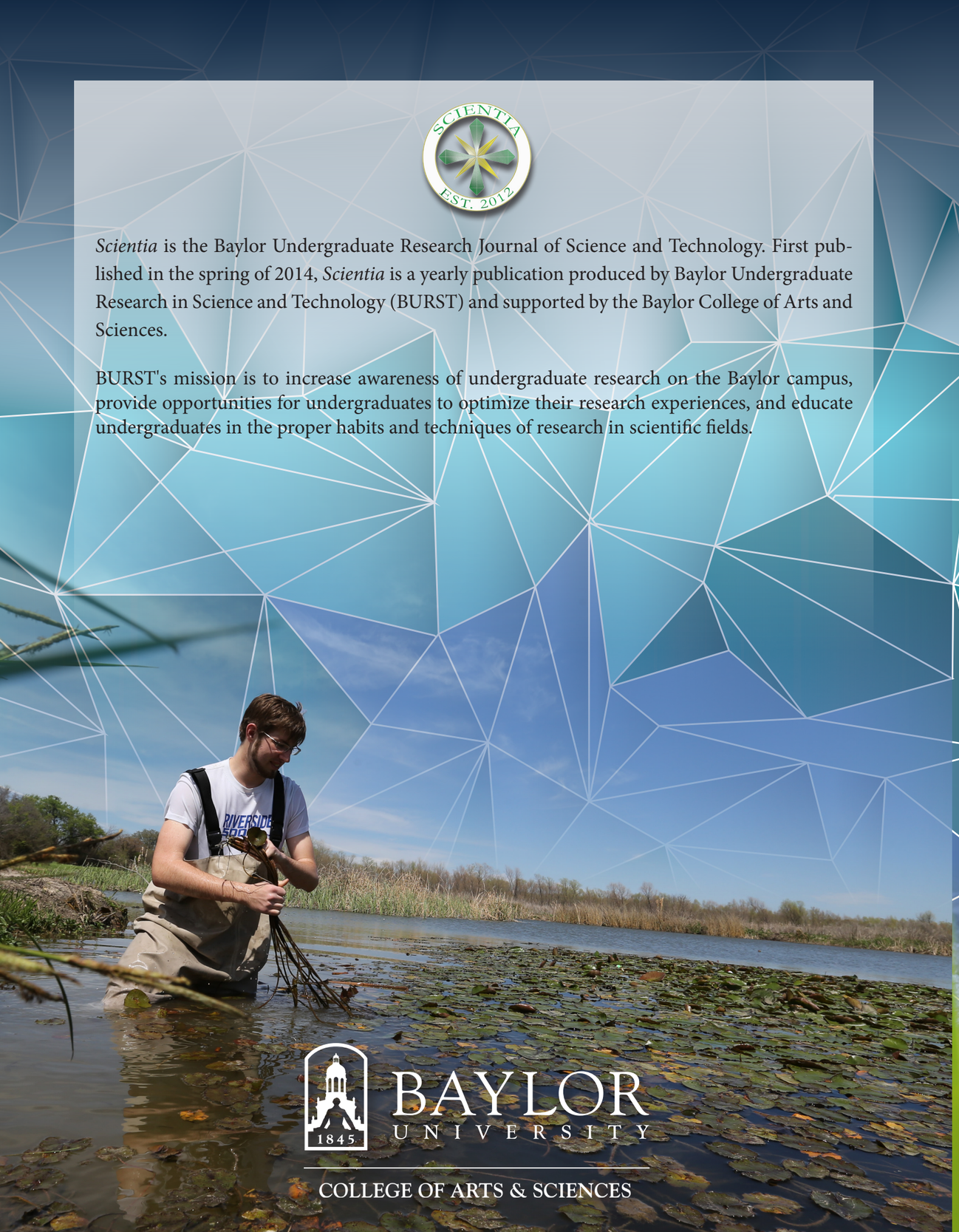

BAYLOR UNIVERSITY

COLLEGE OF ARTS & SCIENCES

Spring 2016

SCIENTIA

The Baylor Undergraduate Research Journal of Science & Technology

College of Arts & Sciences

ISSN 2470-2579

ON THE COVER:

Front Cover: Students from Dr. Marty Harvill's lab record the height of various plants in the Lake Waco Wetlands for their independent research project.
Back Cover: A student from the Harvill Lab uses a net to collect specimen from the Lake Waco Wetlands.

Cover Design by Austin McCrowskie, B.F.A. Graphic Design, 2017

ON THIS PAGE:

Top: Juniors Olivia Hirst and Tyler Pharris adjust the turbine blade of the Cascade Wind Tunnel in the Van Treuren Lab.
Middle: Sophomore Avery Endsley tests specimens in water from Lake Waco in the Harvill Lab.
Bottom: Junior David Le analyzes protein structures in the Shuford Lab.

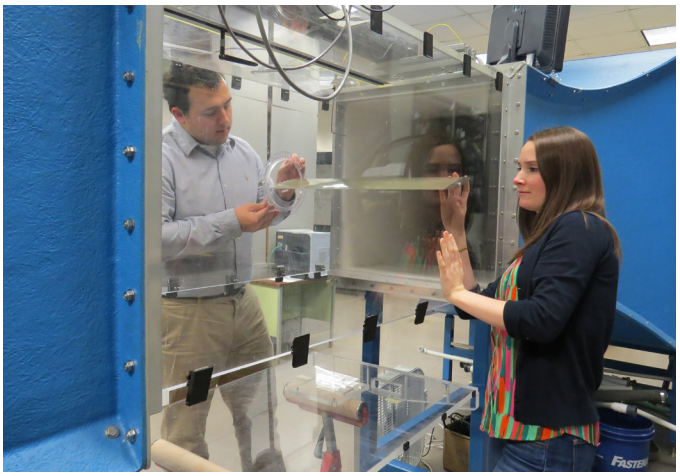

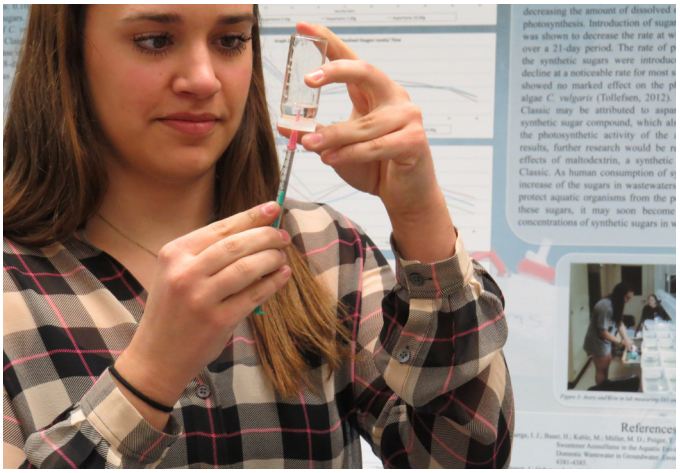

IN THIS ISSUE

Introduction

2015: A Year of Research in Review

Ahsan Ali, Jade Connor, James Courtright, Paul Early, Tanner Hood, David Le, Boyan Leng, Mallory Myers, Aparna Sarode, and Vivianna Wu
Baylor University, Waco, Texas, USA

In 2015, we saw many breakthroughs in science, from the completion of the genome sequencing of the Kennewick Man to new observations of the landscape of the dwarf planet Pluto. Scientific discoveries were made every single day: according to the International Association of Scientific, Technical, and Medical Publishers, approximately 7-9 million articles were published in 2015. The sheer volume of research output in 2015 made it difficult to select which research articles to highlight in our journal. Despite this fact, we chose ten scientific developments that were published in 2015, taking care to highlight a variety of scientific disciplines. While these ten discoveries in no way are the most significant breakthroughs made in 2015 (only time will reveal their significance), they represent some key qualities of good scientific research: collaboration, ingenuity, precision, and perseverance. Through this short introduction to some of the work done by researchers last year, we not only learn about the research being done in the world, but also gain insight into how undergraduate research at Baylor University fits into the greater narrative of modern science.

CRISPR: A New Innovation in Gene Therapy

By utilizing the power of the gene editing enzyme complex CRISPR, several different teams of researchers have been able to alter the genes of mice affected by Duchenne muscular dystrophy.[1] The loaded CRISPR complex can cut away the hindering mutations on the gene that produces dystrophin, allowing the mice to retain the use of their muscles. This technology could potentially help hundreds of thousands of people afflicted with the disease.

For more information, go to: http://www.sciencemag.org/news/2015/12/crispr-helps-heal-mice-muscular-dystrophy

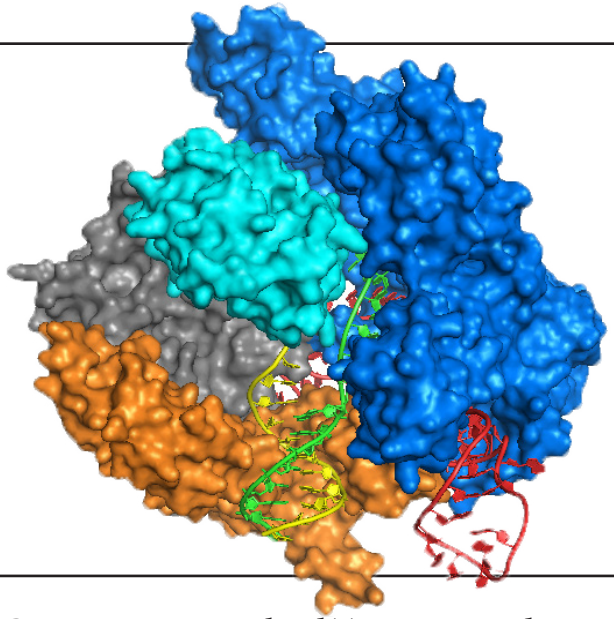

Image Courtesy of Wikimedia Commons Available at https://commons.wikimedia.org/wiki/File:Cas9_Anders_DNA_bound_structure.png

Zika Virus: A New Strain

The Zika virus is spread by bites of infected mosquitoes in the *Aedes* genus. The virus was first identified in the Zika Valley in Uganda and has spread to southern Asia, the Pacific Islands, and the Americas. Infected patients can experience fever, rash, and joint pain. While it is not generally dangerous to children or adults, it can cause great risk for unborn babies. There have been multiple cases of microcephaly in babies of infected mothers, but the mechanism behind this is still unknown.[2] There is currently no vaccination for this virus, but strides have been made to find a vaccination in the upcoming year.

For more information, go to: http://www.who.int/mediacentre/factsheets/zika/en

Cancer-Detecting Blood Test: Improved Diagnostics

A team of researchers at the University of Umea has developed a method of detecting cancer with a blood test.[3] The blood test enables researchers to examine the changes in the RNA of blood platelets induced by tumor cells. In the study, the blood test correctly detected whether or not a patient had cancer 96 percent of the time. This breakthrough brings us one step closer to improving early cancer detection and reducing invasive detection methods.

For more information, go to: http://www.upi.com/Health_News/2015/11/12/Blood-test-can-detect-classify-cancer-in-the-body/5391447346361

Lymphatic Vessels in the Brain: A First Look

Researchers at the University of Virginia School of Medicine have discovered lymphatic vessels in the brain, which have long been thought not to exist.[4] Previously, the mechanisms by which immune cells enter and exit the central nervous system were poorly understood. When asked how these lymphatic vessels remained undetected for so long, the researchers described them as "very well hidden" and in an area difficult to image. The finding has significant implications for the study of neurological diseases such as Alzheimer's, multiple sclerosis, and autism.

For more information, go to: http://neurosciencenews.com/lymphatic-system-brain-neurobiology-2080

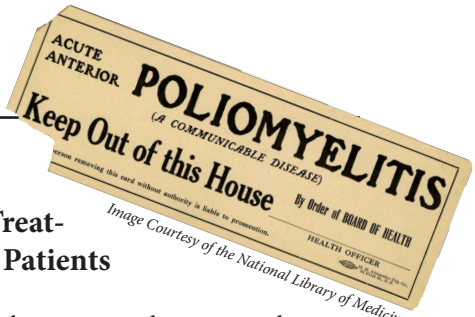

Image Courtesy of the National Library of Medicine

The Periodic Table: The Final Elements

The seventh row of the period table is now complete. Over the past decade, researchers from Japan, Russia, and the United States have discovered elements 113, 115, 117, and 118 by tracking the decay of lighter elements. Although the research itself was not conducted in 2015, the International Union of Pure and Applied Chemistry (IUPAC) officially credited the researchers with their discoveries in December after years of investigation to confirm the findings.[5,6] Now, in 2016, these four elements will be named and begin to appear on periodic tables around the world.

For more information, go to: https://www.sciencenews.org/article/four-elements-earn-permanent-seats-periodic-table

Genetically Engineered Poliovirus: Alternative Treatment Option for Cancer Patients

At Duke University, clinical trials are currently ongoing that utilize genetically engineered poliovirus (PVS-RIPO) as a treatment for recurrent glioblastoma brain tumors. As an oncolytic virus that is administered directly into the tumor, PVS-RIPO targets almost all cancer types by eliciting the human immune response to the infected area.[7] Preliminary findings show no harm to neurons and no risk of PVS-RIPO reverting back to wild type and causing poliomyelitis. This clinical trial, if successful, introduces a new way to treat cancer.

For more information, go to: http://www.cancer.duke.edu/btc/modules/research3/index.php?id=41

Mass Extinction: The Risk Remains

The sixth mass extinction is nearly upon us, but will it be caused by an asteroid or some other natural disaster? According to scientists: it is neither.[8] The cause of the sixth mass extinction is humankind. Through the destruction of ecosystems and resource overuse, man has inadvertently caused a decay of biodiversity that is more rapid than previous extinction events. This extinction event still has the potential to be halted via increased conservation efforts, however, the window of opportunity is quickly closing.

For more information, go to: https://www.washingtonpost.com/news/morning-mix/wp/2015/06/22/the-earth-is-on-the-brink-of-a-sixth-mass-extinction-scientists-say-and-its-humans-fault


Image Courtesy of Dr. Graham Beards
Available at https://commons.wikimedia.org/wiki/Category:Antibiotics#/media/File:M._cat_BSAC.JPG

Teixobactin: The Latest Antibiotic

At the beginning of 2015, through collaboration between numerous German and American scientists, a new antibiotic known as Teixobactin was discovered.[9] Teixobactin is the first new antibiotic developed in the past thirty years, and will be the first in a new class of bacteriacidals. This antibiotic was shown to not display any antibiotic resistance when tested against Methicillin-resistant *Staphylococcus aureus.* Not only does this drug show promise in the age of antibiotic resistance and superbugs, but the iChip technology used to engineer Teixobactin showcases great potential for future landmark drug discoveries.

For more information, go to: http://phenomena.nationalgeographic.com/2015/01/07/antibiotic-resistance-teixobactin

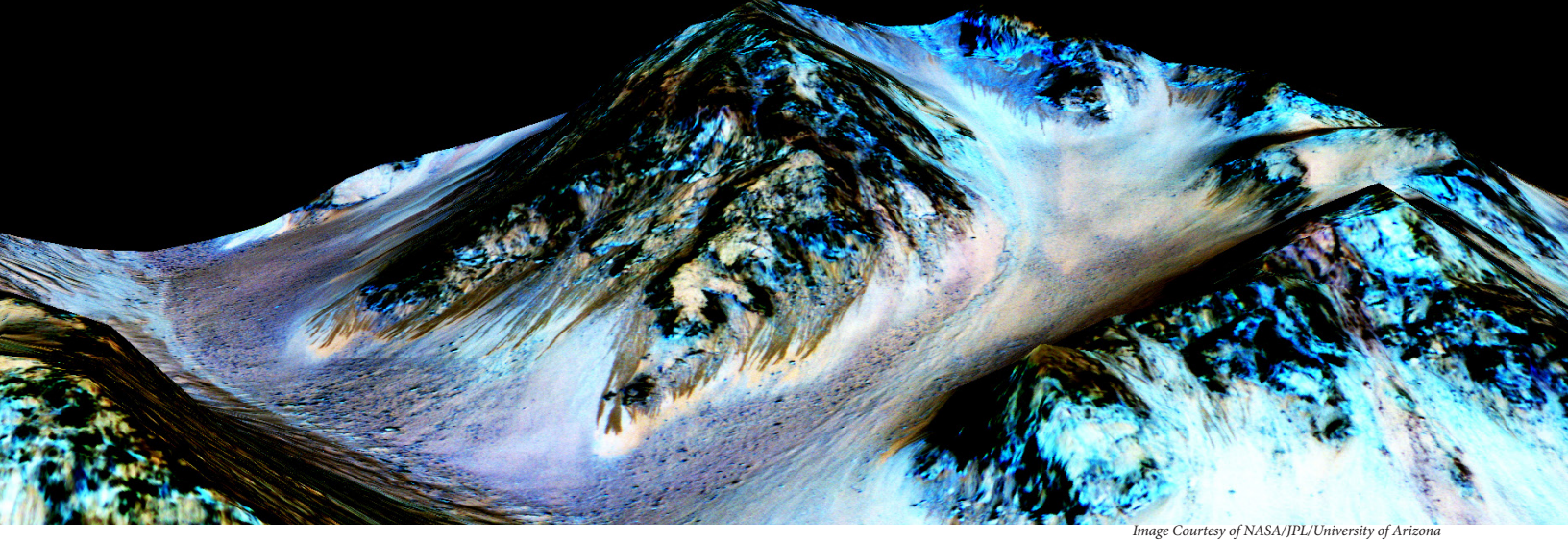

Image Courtesy of NASA/JPL/University of Arizona

Liquid Water on Mars: New Evidence

Since 2011, scientists have seen potentially water-related streaks appear and disappear on the surface of Mars. These streaks appear in the warm seasons, when water is most likely to be in its liquid state, and disappear during the cold season. Recently, scientists have found hydrated salts along these streaks that confirm the original hypothesis that the streaks were formed by water.10 These salts would lower the freezing point of water and provide further evidence for the presence of liquid water on the surface of Mars.

For more information, go to: http://www.nasa.gov/press-release/nasa-confirms-evidence-that-liquid-water-flows-on-today-s-mars

Blocking HIV: A Potential Treatment

HIV now has a potential treatment through gene therapy. By changing the virus' CD4 protein receptor, researchers have prevented HIV from attaching itself to immune cells.[11] This process is achieved by modifying the HIV CD4 protein receptors to CD4-Ig. This test of the new gene therapy is potent in animals, but the effects in humans are still unknown.

For more information, go to: http://www.sciencemag.org/news/2015/02/stopping-hiv-artificial-protein

References

1. Ousterout, D. G.; Kabadi, A. M.; Thakore, P. I.; Majoros, W. H.; Reddy, T. E.; Gersbach, C. A. Multiplex CRISPR/Cas9-based genome editing for correction of dystrophin mutations that cause Duchenne muscular dystrophy. *Nat. Commun.* **2015,** *6,* 6244.
2. Mlakar, J.; Korva, M.; Tul, N.; Popović, M.; Poljšak-Prijatelj, M.; Mraz, J.; Kolenc, M.; Rus, K. R.; Vipotnik, T. V.; Vodušek, V. F.; et al. Zika Virus Associated with Microcephaly. *N. Engl. J. Med.* [Online] **2016**. http://dx.doi.org/10.1056/NEJMoa1600651 (accessed February 14, 2016).
3. Best, M. G.; Sol, N.; Kooi, I.; Tannous, J.; Westerman, B. A.; Rustenburg, F.; Schellen, P.; Verschueren, H.; Post, E.; Koster, J.; et al. RNA-Seq of Tumor-Educated Platelets Enables Blood-Based Pan-Cancer, Multiclass, and Molecular Pathway Cancer Diagnostics. *Cancer Cell.* **2015**, *28* (5), 666–676.
4. Louveau, A.; Smirnov, I.; Keyes, T. J.; Eccles, J. D.; Rouhani, S. J.; Peske, J. D.; Derecki, N. C.; Castle, D.; Mandell, J. W.; Lee, K. S.; et al. Structural and functional features of central nervous system lymphatic vessels. *Nature.* **2015**, *523*, 337-341.
5. Karol, P. J.; Barber, R. C.; Sherrill, B. M.; Vardaci, E.; Toshimitsu, Y. *Discovery of the elements with atomic numbers Z=113, 115 and 117*; IUPAC Technical Report: Pittsburgh, PA, 2016; 139-153.
6. Karol, P. J.; Barber, R. C.; Sherrill, B. M.; Vardaci, E.; Toshimitsu, Y. *Discovery of the elements with atomic number Z=118 completing the 7th row of the periodic table*; IUPAC Technical Report: Pittsburgh, PA, 2016; 155-160.
7. Dobrikova, E. Y.; Broadt, T.; Poiley-Nelson, J.; Yang, X.; Soman, G.; Giardina, S.; Harris, R.; Gromeier, M. Recombinant Oncolytic Poliovirus Eliminates Glioma In Vivo Without Genetic Adaption to a Pathogenic Phenotype. *Mol. Thera.* **2008,** *16* (11), 1865-1872.
8. Ceballos, G.; Ehrlich, P. R.; Barnosky, A. D.; García, A.; Pringle, R. M.; Palmer, T. M. Accelerated modern human-induced species losses: Entering the sixth mass extinction. *Sci. Adv.* **2015**, *1* (7), e1400253.
9. Ling, L. L.; Schneider, T.; Peoples, A. J.; Spoering, A. L.; Engels, I.; Conlon, B. P.; Mueller, A.; Schaberle, T. F.; Hughes, D. E.; Epstein, S.; et al. A new antibiotic kills pathogens without detectable resistance. *Nature.* **2015**, *517* (7535), 455-459.
10. Ojha, L.; Wilhelm, M. B.; Murchie, S. L.; McEwen, A. S.; Wray, J. J.; Hanley, J.; Massé, M.; Chojnacki, M. Spectral evidence for hydrated salts in recurring slope lineae on Mars. *Nat. Geosci.* **2015,** *8,* 829-832.
11. Gardner, M. R.; Kattenhorn, L. M.; Kondur, H. R.; von Schaewen, M.; Dorfman, T.; Chiang, J. J.; Haworth, K. G.; Decker, J. M.; Alpert, M. D.; Bailey, C. C.; et al. AAV-expressed eCD4-Ig provides durable protection from multiple SHIV challenges. *Nature.* **2015,** *519,* 87-91.

Trends of 17β-estradiol Concentrations in the Lake Waco Wetlands

Katie Colanero, Connor Dillon, Alexa Larsen, and Marty Harvill, Ph.D.
Department of Biology, Baylor University, Waco, Texas, USA

Abstract

The objective of this project was to determine the efficiency of the wetlands in the removal of 17β-estradiol from the water supply. The hypothesis was that the concentrations of 17β-estradiol would decrease as water traveled through the Lake Waco Wetlands. The water was collected from the North Bosque River, each cell of the Lake Waco Wetlands, and Lake Waco. After collection, the water's estradiol concentration was tested using an ELISA assay and a Biotek ELx800 Microplate Reader. The results falsified the hypothesis, because there was no statistically significant change in concentration as the water traveled through the Lake Waco Wetlands. This allowed the researchers to conclude that the wetlands did not significantly remove 17β-estradiol from the water supply in this study. Because the wetlands cannot purify the water of this potentially harmful hormone, there are significant ecological ramifications for the surrounding aquatic populations as well as any humans who drink water from this area.

Introduction

This study specifically focused on levels of 17β-estradiol, the primary female sex hormone. A derivative of this hormone is a major component of oral contraceptives and synthetic hormones given to cattle. This is particularly relevant because there are many dairy farms in Texas. Runoff from these farms contains 17β-estradiol and therefore deposits considerable quantities of the hormone in rivers and bodies of water.[1] These elevated levels can cause male fish to develop female reproductive characteristics, affecting fish populations and thus the whole aquatic ecosystem.[2] It is still unknown whether or not these hormones can affect humans over a long period of exposure. This project aimed to determine whether or not the wetlands, as a natural water purifier, would successfully remove the estrogen added to the water by the dairy farm runoff. The hypothesis was that the concentration of estrogen in the water of the Lake Waco Wetlands would decrease as the water traveled through the cells. To answer this question, water was collected from the different cells of the wetlands and assessed with an enzyme-linked immunosorbent assay (ELISA) test. The ELISA assay was used because it was the most sensitive test for detecting the levels of estrogen necessary for a relatively low cost. Most bodies of water contain trace amounts of estrogen, usually in the range of 1 to 80 ng/L, thus a sensitive test was necessary to ensure that the experiment would detect such potentially low levels.[3]

Methods and Materials

Water is pumped into the wetlands from the North Bosque River where it flows in succession through the cells, which are man-made sections of decreasing elevation in the wetlands. Five locations around the wetlands were marked with flags for consistent data collection. These locations were: the entrance of the wetlands at which water is pumped in from the North Bosque river, the exit points of Cells 1, 2, 3, and 4, and the westernmost section of Lake Waco nearest to the wetlands where the water exits.[4] Each week, two 20 mL glass vials were filled at each location, for a total of 12 samples. Once back at the lab, two more 20 mL glass vials were filled with tap water from the lab sink to be used as a control because the tap water has been purified by traditional city water purification methods. The total number of samples was 56 including controls, with fourteen samples collected per week for four weeks. Samples were collected on March 25, April 1, April 8, and April 15, 2015, which will be labeled Weeks 1-4 from here on.

First, 50 µL of six different standard solutions, which were provided with the ELISA test, were added to the wells of the test strips. This provided a standard of comparison each week for the collected samples. The six standards had concentrations of 0, 3, 6, 9, 15, and 25 pg/mL, respectively. 50 µL of each sample, as well as the controls, were then added to their respective wells. The wells provided with the ELISA test contained antibodies to which the estrogen in the water could bind.

Then, 50 µL of E2 antibody solution were added to each well. The wells were covered in parafilm and swirled for 20-30 seconds before incubating for 30 minutes at room temperature. After this incubation period, 50 µL of E2 HRP conjugate solution were added to the individual wells. The wells were again covered with parafilm, mixed and incubated at room temperature, this time for 90 minutes. The antibodies in the solution bound to the estrogen that was already bound to the antibodies in the assay, and produced a chemical reaction.

While the samples were incubating, the wash solution was diluted with deionized water. 10 mL of the concentrated

solution was diluted with 40 mL of deionized water in a 200 mL beaker for a total of 50 mL.

After the incubation period was completed, the liquid contents of the wells were discarded, leaving only the bound antibodies and estrogen. The wells were then rinsed with the diluted wash solution concocted earlier. The rinse procedure included 250 µL of wash solution per well repeated four times. Once clean, 150 µL of substrate/color solution were added to the wells and incubated once more, this time for 20 minutes at room temperature. The color solution reacted with the contents left in the well to produce a color change that was inversely proportional to the concentration of estrogen present in the sample.

When the wells had been incubated for the final time, 100 µL of stop solution were added to the well in the same sequence as the substrate/color solution was added. The degree of color change indicated the degree to which a positive reaction had occurred, which was proportional to the amount of estrogen bound to the antibodies in the well. The plate containing the wells was then taken to a Biotek ELx800 Microplate Reader, located in the Molecular Biosciences Center at Baylor University. An absorbance test was run using a 450 nm filter. This was done within 15 minutes of the completion of the reaction to maximize accuracy. Absorbance spectroscopy was used to obtain an exact measure of the degree of color change. The standard solutions were used to describe the absorption as a function of concentration in order to determine the concentration of estrogen in the samples.

Results

The ELISA assay, when read with a microplate reader, yielded data values that represented the absorbance of the liquid inside each cell when a wavelength of 450 nm was used in the ELx800 microplate reader. The absorbance is an indication of how far the reaction of the estrogen with the estrogen antibody solution was able to proceed, and thus an indicator of the amount of estrogen that was present in the sample. More estrogen present meant the reaction was able to proceed farther, meaning less reactants were left in solution to react with the color solution and the solution absorbed less light. The standards of known concentration were used to create a standard curve for each week. Each standard was divided by the zero standard for that week to obtain a %B/B0 standard value. Any outliers in the standards were excluded in order to create a more accurate best-fit curve. The %B/B0 was then graphed versus the concentration to form a standard curve (Figure 1). A trend line was then fit to the standard curve, yielding a cubic polynomial equation with a y-intercept of 1, because the %B/B0 of the 0 Standard was 1. The cubic polynomial displayed %B/B0 as a function of the estrogen concentration of the sample. Although the data points in the standard curve for week 2 appear to deviate from the best-fit curve more than the standard curves for the other weeks, the R^2 value for the data set was 0.9589, which indicated a close enough fit to include the data.

The data for the samples was divided by the zero standard to obtain %B/B0 sample values, which were then used in conjunction with the cubic trend line equation to obtain the concentration values of the data. The replicates for each cell were then averaged to obtain averages for each cell by week (Figure 2). The data for all the weeks was then averaged to display a monthly average estrogen level for each location in the wetlands (Figures 3 and 4). The data shows trends over time, with high levels of estrogen moving through the wetlands and

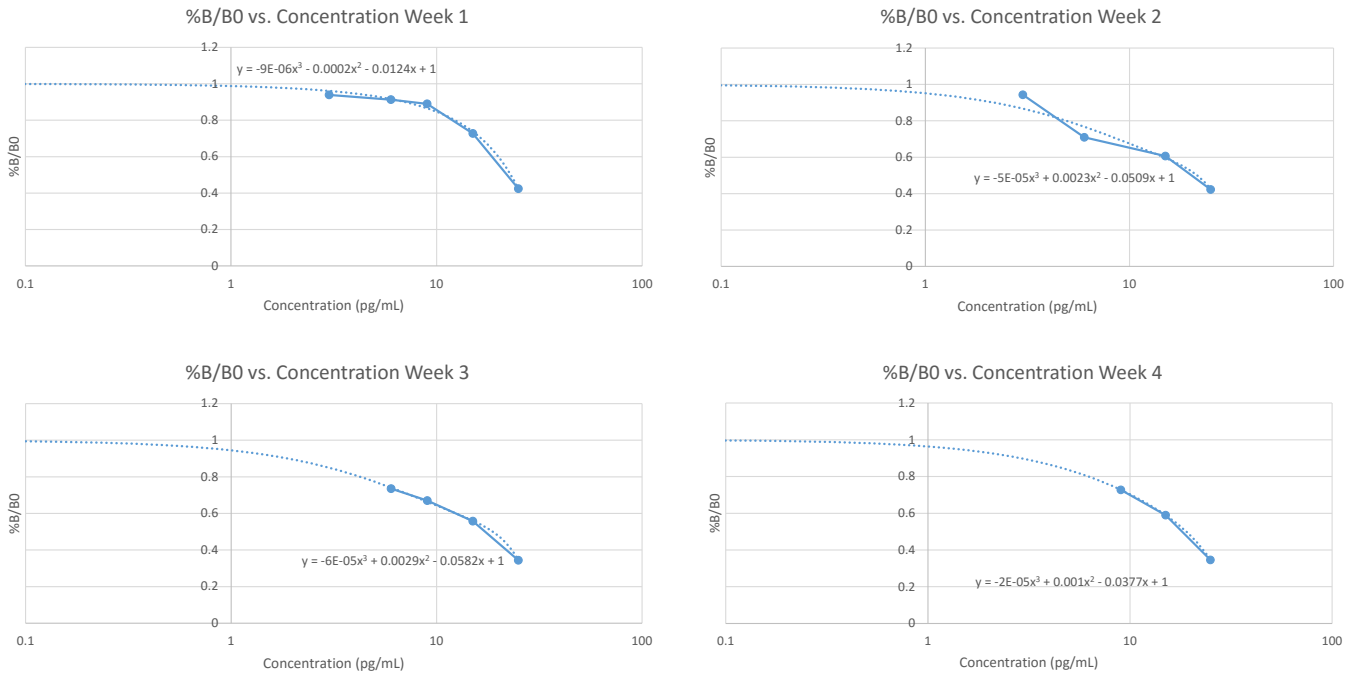

Figure 1. Standard Curves calculated from B%/B0 values v. 17β-estradiol Concentration (pg/mL) by week.The data for Week 3 Standard 2 (6 pg/mL) and Week 4 Standards 2 and 3 (6 pg/mL and 9 pg/mL) were left out of the standard curves because they were outliers.

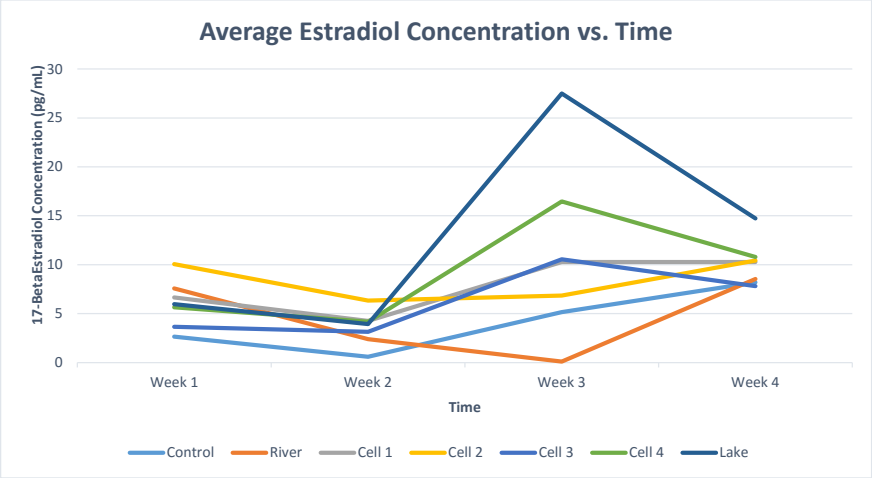

Figure 2. Average 17β-estradiol Concentration (pg/mL) by Sample Location Over Time

Location	Average (pg/mL)	Std. Error
Control	4.143	1.64
River	4.651	2.03
Cell 1	7.864	1.476
Cell 2	8.412	1.063
Cell 3	6.289	1.766
Cell 4	9.267	2.786
Lake	13.028	5.36

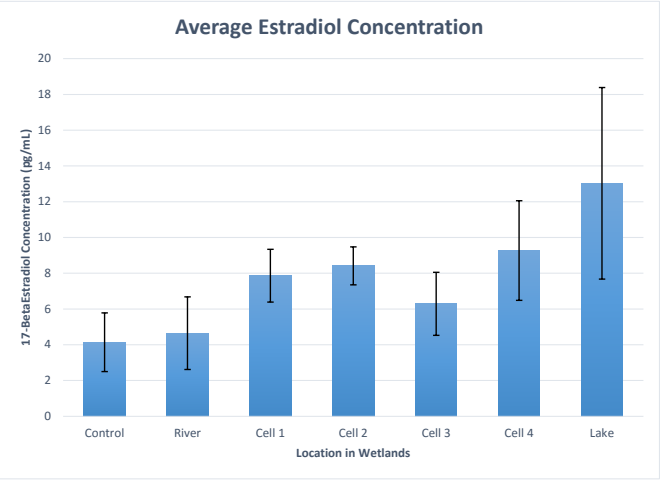

Figures 3 and 4. Average 17β-estradiol Concentration (pg/mL) by Sample Location

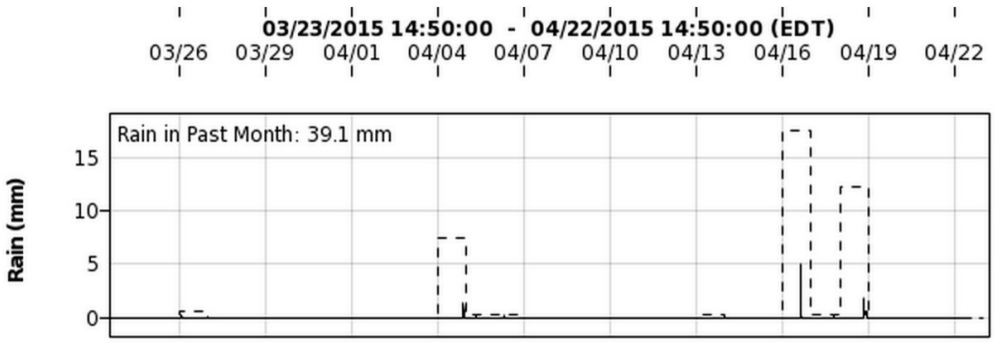

Figure 5. Rainfall in Waco Wetlands from 3/26/15 - 4/22/15

thus appearing in successive cells in successive weeks. However, the overall monthly averages of the estrogen levels in each cell are not statistically significantly different, as the error bars overlap (Figure 4).

Discussion

The working hypothesis was that the wetlands would remove 17β-estradiol from the water due to their water purifying abilities. If the hypothesis had been correct, the estrogen levels would have significantly decreased from the river to Cells 1-4 to the lake. However, the averaged data shows no statistically significant increase or decrease in 17β-estradiol levels from Cell 1 to the lake because the standard error bars overlap (Figure 4). Thus the hypothesis has been falsified; the wetlands do not successfully remove 17β-estradiol from water. These results are consistent with the conclusion that, "wetland treatment did not remove environmental estrogens in the water" found in Xie *et al.*[2] The 17β-estradiol concentration in the river is significantly lower than the rest of the locations, which may be due to the fact that the water is flowing more quickly in the river than in the cells of the wetlands, causing less 17β-estradiol to be retrieved during sample collection.

The samples collected in Week 3 demonstrated a general increase in concentration (Figure 2). The dates between Week 2 and Week 3 were April 1-8, 2015. An examination of the weather data collected by the Waco Wetlands revealed a significant amount of rainfall, around 7 mm, between April 4 and April 7 (Figure 5). Rain causes more soil runoff from the dairy farms that contribute 17β-estradiol to the water, thus estrogen concentration increases after a rainfall. This increase in concentration, however, caused the data to be highly varied, increasing the standard error and possibly masking trends in 17β-estradiol concentration that may have appeared as the water flowed through the wetlands. For example, in week 3, the concentration of estrogen in the lake was calculated to be above 25 pg/mL, which is an extrapolation of the standard curves. Regardless, the data still shows a trend of increased estrogen throughout the wetlands in week 3 due to the rainfall. Furthermore, the spike in estrogen concentration did not appear in cell 2, demonstrating the high variability in estrogen levels especially following rainfall conditions.

The average concentrations of all samples except those collected from the river were significantly higher than the control, which was Baylor University tap water. The concentrations of samples from the lake were especially high, which could suggest that the estrogen accumulated in the more stagnant body of water over time. However, the tap water control, which is water from Lake Waco that is passed through a water purification plant, was relatively low. This trend indicates that at some point during the water purification process that allows the Lake Waco water to become potable, a significant amount of estrogen is removed. Further investigation is needed to determine how the estrogen is removed and whether or not the 4.143 pg/mL concentration of 17β-estradiol in the tap water (Figure 3) have had or could later have harmful effects in human and animal populations.

This proposal is significant because of its ecological implications. According to Zheng *et al.*, "In vitro studies have shown that low concentrations of steroid estrogenic hormones... can adversely affect the reproductive biology of aquatic wildlife."[5] Additionally, Kidd *et al.* found that "Male fishes downstream of some wastewater outfalls [display]… feminization [that] has been attributed to the presence of estrogenic substances such as natural estrogens [estrone or 17β-estradiol (E2)]."[2] These negative effects impact the entire wetland community because changes in fish population have ramifications on the populations of both their predators and their prey. Further studies could examine whether or not these elevated levels of estrogen in water supplies could also have effects in human populations as a result of long-term exposure.

Acknowledgments

Baylor University Biology Department; Ms. Nora Schell; Lake Waco Wetlands; Abraxis Kits; URSA; Hao Wu, Ph.D. Candidate; Molecular Biology Center at Baylor University; and John Bowersox.

References

1. Cavallin, J. E.; Durhan, E. J.; Evans, N.; Jensen, K. M.; Kahl, M. D.; Kolpin, D. W.; Kolodziej, E.P.; Foreman, W. T.; LaLone, C. A.; Makynen, E. A.; et. al. Integrated assessment of runoff from livestock farming operations: Analytical chemistry, in vitro bioassays, and in vivo fish exposures. *Environ. Toxicol. Chem.* / SETAC0. **2014**, *33*(8), 1849–1857.

2. Kidd, K. A.; Blanchfield, P. J.; Mills, K. H.; Palace, V. P.; Evans, R. E.; Lazorchak, J. M.; Flick, R. W. Collapse of a fish population after exposure to a synthetic estrogen. *Proc. Nat. Acad. Sci.* **2007**, *104*(21), 8897–8901.

3. Xie, L.; Sapozhnikova, Y.; Bawardi, O.; Schlenck, D. Evaluation of wetland and tertiary wastewater treatments for estrogenicity using in vivo and in vitro assays. *Arch. Environ. Contam. Toxicol.* **2004**, *48*, 81-86.

4. City of Waco Texas. Lake Waco Wetlands: Frequently Asked Questions. http://www.waco-texas.com/cms-wetlands/page.aspx?id=321 (accessed Feb 27, 2016).

5. Zheng, W.; Li, X.; Yates, S. R.; Bradford, S. A. Anaerobic Transformation Kinetics and Mechanism of Steroid Estrogenic Hormones in Dairy Lagoon Water. *Environ. Sci. Technol.* **2012,** *46*(10), 5471–5478.

The Effect of Synthetic Sugars on the Photosynthetic Activity of *Chlorella vulgaris*

Erin Ahrberg, Daniel Berry, Avery Endsley, Marty Harvill, Ph.D., and Jack Tubbs, Ph.D.
Department of Biology, Baylor University, Waco, Texas, USA

Abstract

Concentrations of synthetic sugars in wastewaters have increased due to human inability to absorb these artificial compounds and the incomplete removal of these compounds in wastewater treatment plants.[1-5] The effect of these synthetic sugars on other aquatic organisms remains unknown. The question was asked how sugars, both natural and artificial, comparatively affect the photosynthetic activity of *Chlorella vulgaris.* In 15 separate containers of a 2.00 L solution, the effect of the sugars aspartame, acesulfame-potassium, sucralose, Equal Classic, and pure cane sugar on algal growth was observed. Each sweetener was compared at 3 different amounts: 0.10 g, 1.00 g, and 10.00 g, and to a control containing no added sugar. Significant detrimental effects on the photosynthetic activity of *Chlorella vulgaris* were observed due to the added synthetic sugars. This was graphed as the percent change in the dissolved oxygen (mg/L) over a 3-week period. All added sugars showed significant changes in the percent change of dissolved oxygen from the baseline present in the sample at week 3 at amounts of 0.10 g and 1.00 g. This preliminary study may prove important in explaining the effects of synthetic sugars as these values continue to increase in wastewater areas.

Introduction

Synthetic sugars have been observed in various wastewater and watershed areas, yet their effect on aquatic organisms is still not fully understood.[3-4, 6-8] *Chlorella vulgaris* is a dominant algal species found in areas similar to the Lake Waco Wetlands, where the culture water in this experiment was collected.[9] In this experiment, *Chlorella vulgaris* represents aquatic organisms being affected by the increased concentration of synthetic sugars in the habitat.

We hypothesized that synthetic sugars, specifically acesulfame-potassium, would show a more detrimental effect on the photosynthetic activity of the algae than the naturally occurring pure cane sugar. The research consisted of measuring the effect of each aspartame, acesulfame-potassium, sucralose, Equal Classic, and pure cane sugar on the photosynthetic activity of *Chlorella vulgaris* in comparison to the control containing no added sugar.

This study focuses on acesulfame-potassium because of its presence in wastewater areas. There have not been sufficient studies to conclusively state the effect acesulfame-potassium has on organisms in the environment, but it has shown possible impact on aquatic ecosystems due to its phototoxicity.[3, 4] Acesulfame-potassium is approved by the United States Food and Drug Administration for consumption and does not consistently break down under extreme conditions.[10] One study observed 10 different wastewater treatment plants where acesulfame-potassium was consistently detected at 12-46 µg/L.[7] Sucralose and aspartame are detected at similar levels in wastewaters.[3-4, 6, 8, 11] The persistence of these synthetic sugars formed the basis of this experiment.

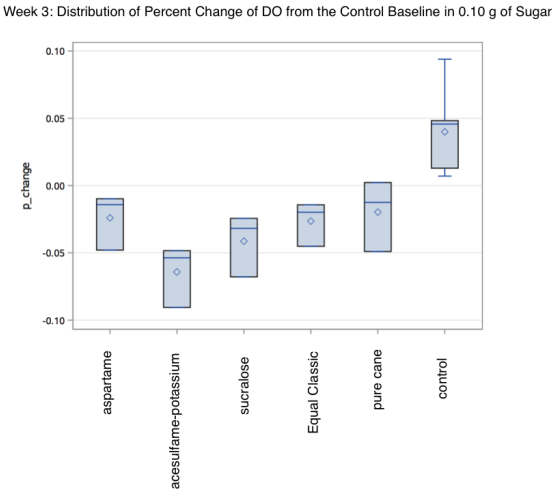

Figure 1. The distribution of percent change (p_change) of dissolved oxygen from the control baseline in 0.10 g of the sugars

Week 3: Comparison of all sugars against control at 0.10 g				
Sugar Comparison	Difference between Means	Simultaneous 95% Confidence Limits		Comparisons significant at the 0.05 level
pure cane - control	-0.05967	-0.10738	-0.01196	***
aspartame - control	-0.06392	-0.11163	-0.01621	***
Equal Classic - control	-0.06636	-0.11407	-0.01865	***
sucralose - control	-0.08128	-0.12899	-0.03357	***
acesulfame-potassium - control	-0.10414	-0.15185	-0.05643	***

Figure 2. This table shows significant differences in the comparison the effect sugars had on the percent change of dissolved oxygen from the control baseline at 0.10 g.

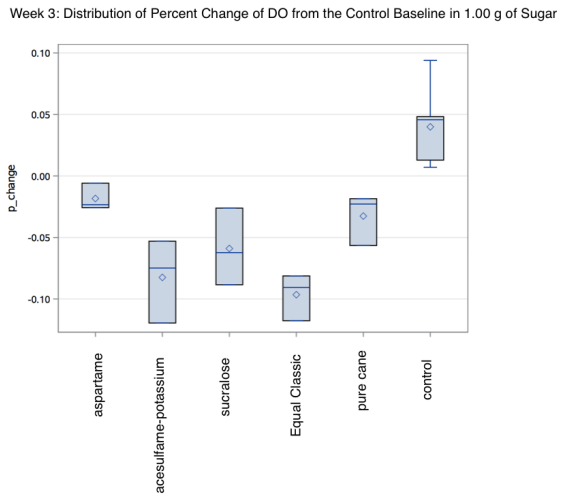

Figure 3. The distribution of percent change (p_change) of dissolved oxygen from the control baseline in 1.00 g of the sugars

Week 3: Comparison of all sugars against control at 1.00 g				
Sugar Comparison	Difference between Means	Simultaneous 95% Confidence Limits		Comparisons significant at the 0.05 level
aspartame - control	-0.05825	-0.10826	-0.00824	***
pure cane - control	-0.07253	-0.12254	-0.02252	***
sucralose - control	-0.09889	-0.14890	-0.04888	***
acesulfame-potassium - control	-0.12239	-0.17240	-0.07238	***
Equal Classic - control	-0.13645	-0.18646	-0.08644	***

Figure 4. This table shows significant differences in the comparison the effects the sugars had on the percent change of dissolved oxygen from the control baseline at 1.00 g.

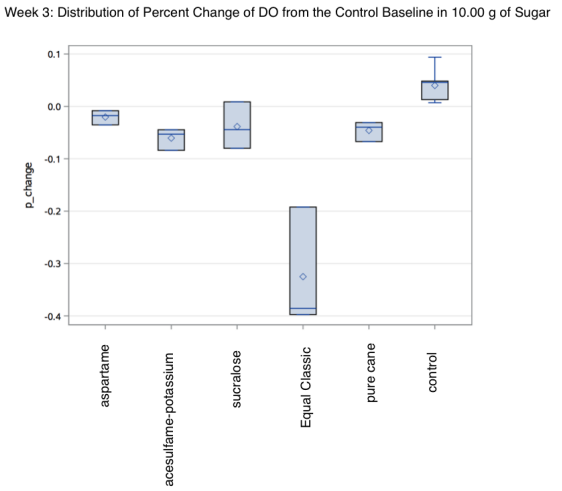

Figure 5. The distribution of percent change (p_change) of dissolved oxygen from the control baseline in 10.00 g of the sugars

Week 3: Comparison of all sugars against control at 10.00 g				
Sugar Comparison	Difference between Means	Simultaneous 95% Confidence Limits		Comparisons significant at the 0.05 level
aspartame - control	-0.06027	-0.14809	0.02755	
sucralose- control	-0.07848	-0.16630	0.00933	
pure cane - control	-0.08581	-0.17363	0.00200	
acesulfame-potassium - control	-0.10043	-0.18825	-0.01262	***
Equal Classic - control	-0.36495	-0.45277	-0.27714	***

Figure 6. This table shows significant differences in the comparison the effects the sugars had on the percent change of dissolved oxygen from the control baseline at 10.00 g.

Methods and Materials

Analytical standards of sugars were acquired. Aspartame and sucralose were purchased from NuSci. The brands for C&H Pure Cane and Equal Classic, respectively, were used. Acesulfame-potassium was purchased through "Prescribed For Life." Eighteen rectangular transparent plastic containers from Sterilite were used to contain the cultured algal solution, which consisted of water from the Lake Waco Wetlands, Alga-Gro Freshwater Medium from Carolina Biological, and a *Chlorella vulgaris* suspension from Ward's Science. The concentration of dissolved oxygen (mg/L), was measured using a Vernier Optical DO probe.

Each of the 18 containers was filled with 2.00 L of water, 50.00 mL of medium, and 100 µL of *Chlorella vulgaris* suspension. After one week, 3 of the 18 containers served as controls while the remaining 15 contained one specific type of sugar at three different amounts: 0.10 g, 1.00 g, and 10.00 g. The concentration of dissolved oxygen (mg/L) and the fluorescence were recorded at equal intervals 3 times a week.

Results

The statistical graphs present a comparison of the effect the added sugars had on the photosynthetic activity, represented as the average percent change in the dissolved oxygen (mg/L) from the baseline, in the water sample. The baseline is the change in the concentration of dissolved oxygen in the control. The significant variance observed for each amount of all five sugars against the control at week 3 is presented in the Figures 2, 4, and 6. Statistical analysis is used to determine the effect that added sugars have on the photosynthetic activity by considering the percent change in the dissolved oxygen (mg/L), from the baseline. Each of the five sugars used similar concentration levels and are compared against a zero-dose placebo control as given in the water sample. Dunnett's test was used to determine if the mean percent change for the sugars have a significant reduction in dissolved oxygen (mg/L) when compared with the water control group.[12] The statistical results for the respective level of amounts (0.1 g, 1.0 g, and 10.0 g) are given in Figures 2, 4, and 6 with the accompanying graphs given in Figures 1, 3, and 5. Figures 1, 3, and 5 show the distributions of average percent change in the dissolved oxygen (mg/L) exhibited by the various synthetic sugars.

As shown in Figures 2, 4, and 6, the percent change of dissolved oxygen significantly decreased for acesulfame-potassium and Equal Classic at all added amounts. Additionally, aspartame, sucralose, and pure cane sugar at added amounts of 0.10 g and 1.00 g resulted in significant decreases in the percent change of dissolved oxygen at the 0.05 confidence level. The percent change of dissolved oxygen is directly related to the amount of oxygen being produced by photosynthetic activity of the algae. Therefore, the significant decreases in the percent change of dissolved oxygen indicates that there was a significant decrease in the photosynthetic activity of the algae when exposed to the varying amounts of synthetic sugars.

Discussion

The data indicates that all of the synthetic sugars as well

as pure cane sugar had a detrimental effect on the photosynthetic activity of *Chlorella vulgaris*, with acesulfame-potassium and Equal Classic showing significant effects at all added amounts. Aspartame, sucralose, and pure cane sugar did not show significant decreases in the percent change of dissolved oxygen from the control baseline at 10.00 g. Aspartame, sucralose, and pure cane sugar did not produce significant variance at 10.00 g, which may be due to the extreme decrease that occurred in Equal Classic in comparison to the control. Further statistical analysis may be examined to reveal whether or not the changes caused by aspartame, sucralose, and pure cane sugar at 10.00 g was significant.

Introduction of sugars, both natural and synthetic, was shown to decrease the rate at which photosynthesis occurred over a 21-day period, as represented by the decreasing amount of dissolved oxygen, a direct byproduct of photosynthesis. The decrease in the percent change from the baseline that occurs at week 3 may be attributed to the introduction of synthetic sugars, or to other growth factors. It is possible that this is the result of density-dependent inhibition or competitive exclusion that causes the death of a percentage of the algae due to the lack of resources to support exponential growth. Other studies have shown the photosynthetic rate of *Chlorella vulgaris* being inhibited by the presence of glucose.[13] The uptake of different sugars by plants varies by many factors including the natural presence of that sugar in the plant or algae and the concentration of the added sugar.[14] The rate of photosynthesis declined when the synthetic sugars were introduced. Sucralose has been proven as a competitive inhibitor of ShSUT1 in tests on sugarcane and has been shown to cause sublethal effects on *Daphnia magna.*[15, 16] In other studies, sucralose has not been proven to inhibit sucrose uptake or plant growth rate.[17] The effects shown by Equal Classic may be attributed to one of the components of the synthetic sugar compound or on the compound as a whole.

For more conclusive results, further research would be required to test the effects of maltodextrin, a synthetic sugar also found in Equal Classic. Expansion of this research may include determining what specific component in synthetic sugars is detrimental and at what amount these sugars start showing a detrimental effect. As human consumption of synthetic sugars increases, their concentrations in wastewater areas will increase as they pass unabsorbed through digestion.[2] In order to protect aquatic organisms from the potentially harmful effects of these sugars, it may soon become necessary to monitor the concentrations of synthetic sugars in water reserves.

Acknowledgments

We would like to thank the Lake Waco Wetlands, the Baylor University Department of Biology, Nick Bellacicco, Hao Wu, and Tim Bowersox for their help and contribution to our research.

References

1. Mead, R. N.; Morgan, J. B.; Avery, G. B.; Kieber, R. J.; Kirk, A. M.; Skrabal, S. A.; Willey, J. D. Occurrence of the Artificial Sweetener Sucralose in Coastal and Marine Waters of the United States. *Mar. Chem.* **2009**, *116*, 13-17.
2. Roberts, A.; Renwick, A. G.; Sims, J.; Snodin, D. J. Sucralose Metabolism and Pharmacokinetics in Man. *Food Chem. Toxicol.* **2000**, *38*, S31-S41.
3. Sang, Z.; Jiang, Y.; Tsoi, Y.; Leung K. S. Evaluating the Environmental Impact of Artificial Sweeteners: A Study of Their Distributions, Photodegradation and Toxicities. *Water Res.* **2014**, *52*, 260-274.
4. Scheurer, M.; Storck, F. R.; Brauch, H. J.; Lange, F. T. Performance of Conventional Multi-Barrier Drinking Water Treatment Plants for the Removal of Four Artificial Sweeteners. *Water Res.* **2010**, *44*, 3573-3584.
5. Shankar, P.; Ahuja, S.; Sriram, K.; Non-Nutritive Sweeteners: Review and Update. *Nutrition*. **2013**, *29*, 1293-1299.
6. Berset, J.; Ochensenbein, N. Stability Considerations of Aspartame in the Direct Analysis of Artificial Sweeteners in Water Samples using High-Performance Liquid Chromatography-Tandem Mass Spectrometry (HPLC-MS/MS). *Chemosphere.* **2012**, *88*, 563-569.
7. Buerge, I. J.; Buser, H.; Kahle, M.; Müller, M. D.; Poiger, T. Ubiquitous Occurrence of the Artificial Sweetener Acesulfame in the Aquatic Environment: An Ideal Chemical Marker of Domestic Wastewater in Groundwater. *Environ. Sci. Technol.* **2009**, *43*, 4381-4385.
8. Mawhinney, D. B.; Young, R. B.; Vanderford, B. J.; Borch, T.; Snyder, S. A. Artificial Sweetener Sucralose in U.S. Drinking Water Systems. *Environ. Sci. Technol.* **2011**, *45,* 8716-8722.
9. Izaguirre, I.; O'Farrell, I.; Unrein, F.; Sinistro, R.; dos Santos Afonso, M.; Tell, G. Algal Assemblages Across a Wetland, from a Shallow Lake to Relictual Oxbow Lakes (Lower Paraná River, South America). *Hydrobiologia*. **2004**, *511*, 25-36.
10. Subedi, B.; Kannan, K.; Fate of Artificial Sweeteners in Wastewater Treatment Plants in New York State, U.S.A. *Environ. Sci. Technol.* **2014,** *48,* 13668-13674.
11. Tollefsen, K. E.; Nizzetto, L.; Huggett, D. B. Presence, Fate, and Effects of the Intense Sweetener Sucralose in the Aquatic Environment. *Sci. Total Environ.* **2012**, *438*, 510-516.
12. Dunnett C. W. A Multiple Comparison Procedure for Comparing Several Treatments with a Control *J. Am. Stat. Assoc.* **1995**, *50*, 1096–1121.
13. Martinez, F.; Orús, M. I. Interactions Between Glucose and Inorganic Carbon Metabolism in Chlorella vulgaris Strain UAM 1011. *Plant Physiol.* **1991**, *95*, 1150-1155.
14. Grant, B. R.; Beevers, H. Absorption of Sugars by Plant Tissues. *Plant Physiol.* **1964**, *39*, 78-85.
15. Reinders, A.; Sivitz, A. B.; Hsi, A.; Grof, C. P.; Perroux, J. M.; Ward, J.M. Sugarcane ShSUT1: Analysis of Sucrose Transport Activity and Inhibition by Sucralose. *Plant Cell Environ.* **2006**, *29*, 1871-1880.
16. Wiklund, A. E.; Adolfsson-Erici, M.; Liewenborg, B.; Gorokhova, E. Sucralose Induces Biochemical Responses in Daphnia magna. *Plos One.* **2014**, *9,* 1-6.
17. Soh, L.; Connors, K. A.; Brooks, B. W.; Zimmerman, J. Fate of Sucralose through Environmental and Water Treatment Processes and Impact on Plant Indicator Species. *Environ. Sci. Technol.* **2011**, *45*, 1363-1369.

An Empirical Estimation for the Distribution of rth Record Time

Jonathan C. Myers
Department of Statistical Science, Baylor University, Waco, Texas, USA

Abstract

Compared to other topics within statistics, research on record values is relatively recent. There is currently no method for modeling record times for various distributions based on a single parameter. This paper proposes a new probability distribution which can be used to model the rth record times from a set of normally distributed data with a single parameter, r. This distribution was derived through a simulation of independent standard normal data which was run until the 10th record was observed. Several of the graphs of the record times are shown. A goodness of fit analysis was performed to compare the logarithm of the record times with a lognormal distribution, the transformation of which is how this probability distribution was derived. Also proposed in this paper are common percentiles for several r values, a numerical estimation for the median of the distribution, and an estimator for r. The median and estimator for r were computed, and the bias of their results is shown.

Introduction

The majority of research in record statistics today is built upon work done by K. N. Chandler in 1952.[1] This research sought to determine whether the number of iterations it takes to reach the rth record fits a distribution, so that future problems could predict intervals of record times for the rth record achieved. The amount of time it takes to simulate records from normally distributed data past the 10th record is large, oftentimes requiring greater than 10 million simulated values; thus, being able to calculate confidence intervals could be a helpful tool in order to determine approximately how many data values are necessary in order to achieve the rth record.

In this paper, a record is defined as the highest value in a set of given data, and a record time is the number of iterations it takes to reach a record from the start of data collection. Because the first data point measured is the highest data point in the set, we will consider the first data point measured to be the 1st record.

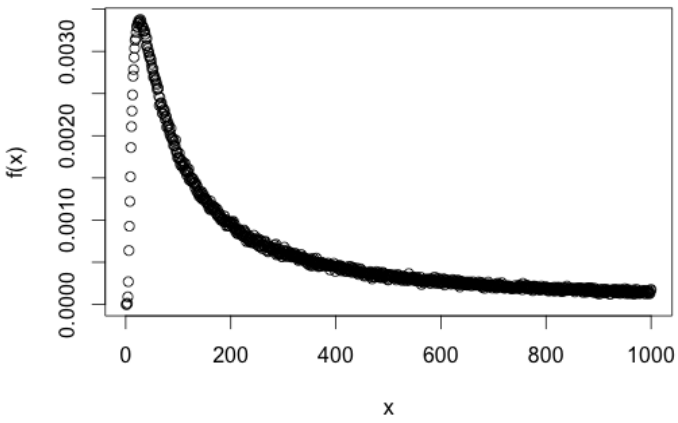

Figure 1. Record Time Probability Distribution for 7th Record

Methods

A simulation study was performed in R, the statistical computing software, using standard normal data. The record times to reach the rth record were saved for records 1 through 10 across 46,099 sets of data. When fitting the data, it was observed that the natural log of the data fits the lognormal distribution, with $\mu \to \ln(r-1)$ and $\sigma \to \sqrt{\frac{1}{r}}$. From this, we performed an inverse log transformation on the lognormal probability distribution function and substituted these values in for μ and σ to reach a new probability distribution, which we call the Myers Distribution.

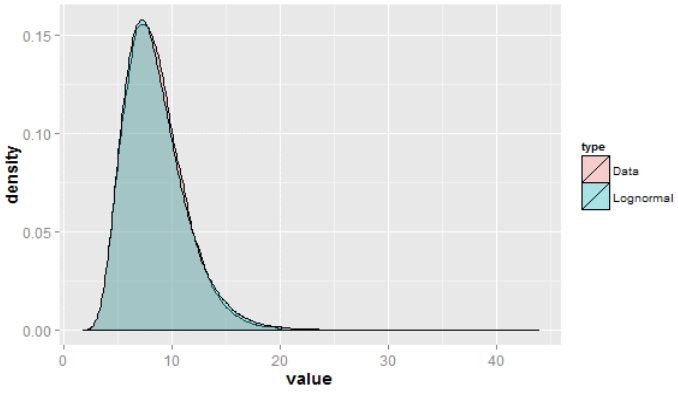

Figure 2. Log of Record Times for 9th Record. Heavy overlap indicates that this distribution follows closely with the data.

γ	r=3	r=4	r=5	r=6	r=7	r=8	r=9	r=10
.005	2	2	4	6	10	17	30	54
.010	3	3	5	7	12	22	40	75
.050	4	4	7	13	25	50	102	211
.100	5	5	10	19	40	86	185	404
.500	7	20	55	148	403	1097	2981	8103
.900	62	296	1207	4615	16967	60611	211817	727421
.950	153	919	4220	17782	71147	274192	1027108	3762128
.990	1096	14434	82818	410435	1895396	8311030	35058919	143472041
.995	2120	50426	316215	1640829	7915219	36118536	158144713	670415326

Table 1: CDF Values

	r=3	r=4	r=5	r=6	r=7	r=8	r=9	r=10
Median	7.3891	20.0855	54.5982	148.4132	403.4288	1096.6330	2980.9580	8103.084

Table 2: Median Values

Tables 1 and 2. Cumulative Distribution Function (CDF) values and median values of various record times. For a given value of r, γ is the probability that the number of iterations it takes to reach the next highest record is less than or equal to the value shown.

Results

Distribution

The lognormal probability distribution function is given by:

$$f(x)=\frac{1}{x\sqrt{2\pi\sigma^2}}e^{\frac{-(\ln x-\mu)^2}{2\sigma^2}}$$

The inverse log transformation follows:

$$f(x)=\frac{1}{lnx\sqrt{2\pi\sigma^2}}e^{\frac{-(\ln\ln x-\mu)^2}{2\sigma^2}}\cdot\frac{1}{x}$$

Substituting in $\mu=\ln(r-1)$ and $\sigma=\sqrt{\frac{1}{r}}$:

$$f(x)=\frac{1}{xlnx\cdot\sqrt{2\pi\sqrt{\frac{1}{r}}^2}}\cdot e^{\frac{-(\ln(\ln x)-\ln(r-1))^2}{2\sqrt{\frac{1}{r}}^2}}$$

$$f(x)=\sqrt{\frac{r}{2\pi}}\cdot\frac{1}{x\ln x}\cdot\sqrt{\frac{r-1}{\ln x}}^{r\cdot\ln\frac{\ln x}{(r-1)}},x\geq 2$$

(Myers Distribution)

Figure 1 displays the new probability distribution for r=7. Figure 2 shows the similarity between the lognormal distribution and the log of the sample data for r=9.

Moments

In order to calculate $E[Y^k]$, where Y~Myers(r), we know $Y=e^X$ where X~lognormal($\mu=\ln(r-1)$ and $\sigma=\sqrt{\frac{1}{r}}$). So,

$E[Y^k]=E[e^{Xk}]$, which is the Moment Generating Function for the lognormal distribution. Because the lognormal distribution has no moment generating function, the moments for the Myers Distribution are not finite.

Cumulative Distribution Function

The integral of the probability density function is not defined; however, percentiles can be calculated when r is known. Table 1 shows the percentiles for r > 1. It does not make sense to arrive at the r^{th} record in x iterations if x is less than r (i.e., reaching the 4^{th} record after only 3 data values); therefore, for the lower values of r where this is observed, it may be a valuable practice to substitute r for those x values.

Median

The logarithm is a monotonic function. Because the median for the lognormal distribution is known to be e^{μ}, we know the median for the Myers Distribution can be evaluated as $e^{e^{\ln(r-1)}}$, or e^{r-1}.Table 2 displays the values of the evaluated median, which can be compared to the cumulative distribution function value for γ=0.500.

Estimators

Because this distribution is a transformation of the Normal Distribution, and we know the estimator for μ for the Normal Distribution, we can calculate the estimator for this distribution.

r	$\hat{r}$
2	2.1176
3	3.1184
4	4.1057
5	4.9244
6	5.7769
7	6.7294
8	7.8803
9	8.9054
10	9.9918

Table 3. Estimator Results

$$Y_i = \ln \ln X_i, i = 1, \ldots, n$$

where Y is normally distributed.

$\overline{Y} = \frac{\sum_{i=1}^{n} Y_i}{n}$ is an unbiased estimator for μ, and μ = ln(r−1).

$$\overline{Y} = \ln(\hat{r} - 1)$$

$$e^{\overline{Y}} = \hat{r} - 1$$

$$\hat{r} = e^{\overline{Y}} + 1$$

$$\hat{r} = e^{\frac{\sum_{i=1}^{n} Y_i}{n}} + 1$$

$$\hat{r} = \exp\{\frac{1}{n} \cdot \ln \prod_{i=1}^{n} [\ln X_i]\} + 1$$

$$\hat{r} = \prod_{i=1}^{n} [\ln X_i]^{\frac{1}{n}} + 1$$

Estimator results from an independent, smaller sample of 100 observations is shown in Table 3.

Asymptotic Results

It should be noted that as $r \to \infty, \mu \to \infty$ and $\sigma \to 0$.

Conclusion

Although the distribution proposed in this paper surrounding this research was focused on normally distributed data in which the mean and standard deviation remain constant, further research could be performed to consider the distribution of record times for other probability distributions, as well as for distributions in which the parameters are not constant (such as in weather or sports data, where the population mean increases over time). This could help to potentially analyze the number of days it will take to reach the next record high temperature in a given city, for instance.

Nomenclature

r^{th} record time	Distribution changes based on the value of r
μ	Mean of the distribution
σ	Standard deviation of the distribution
γ	Probability that the record time is less than or equal to a given value based on r
$E[Y^k]$	Moments of the probability distribution
$\hat{r}$	Estimator for r calculated from simulated data

Acknowledgments

I would like to thank Dr. Jeanne Hill of the Department of Statistical Science at Baylor University for her suggestions.

References

1. Chandler, K. N. The Distribution and Frequency of Record Values. *J. R. Stat. Soc*. **1952**, *14*, 220–228.
2. Galambos, J. *The Asymptotic Theory of Extreme Order Statistics;* Wiley: New York, 1978.
3. Meinhold, R. J.; Singpurwalla, N. D. A Kalman-Filter Smoothing Approach For Extrapolations in Certain Dose–Response, Damage-Assessment, and Accelerated-Life-Testing Studies. *Am. Stat*. **1987**, *41*, 101–106.
4. Nevzorov, V. B. Records. *Theory Probab. Appl.* **1987**, *32*, 201–228.
5. Resnick, S. I. Limit Laws for Record Values. *Stoch. Proc. Appl.* **1973**, *1*, 67–82.
6. Shorrock, R. W. On Record Values and Record Times. *J. Appl. Prob.* **1972**, *9*, 316–326.
7. Yang, M. C. K. On The Distribution of the Inter-Record Times in an Increasing Population. *J. Appl. Prob.* **1975**, *12*, 148.

Original Research

How Varying Reynolds Numbers and Turbulence Intensities Affect Flow Separation on Turbine Blades

Tyler M. Pharris, Olivia E. Hirst, and Kenneth W. Van Treuren, Ph.D.
Department of Mechanical Engineering, Baylor University, Waco, Texas, USA

Abstract

Modern jet engines experience fluid temperatures that would normally melt many of their components. The high-pressure turbine eliminates this problem by cooling the blades with internal channels of air and producing a film of relatively cool air on the surface of the blades. The higher temperatures are also experienced by the low-pressure turbine but it does not utilize any cooling technologies. The problems created by high temperatures in the low-pressure turbine are compounded by flow separation, ultimately causing large thermal stresses on the blades. At low altitudes, when the Reynolds number is high, fluid flow in the low-pressure turbine tends to stay attached to the surface of the blades. However, at the high altitudes reached during cruise, the low Reynolds number (25,000 to 200,000) flow frequently separates from the suction surface of the blades. These experiments test how the flow field of the L1A turbine blade changes as the Reynolds number and turbulence intensity vary within the Baylor University Cascade Wind Tunnel (BUC). Quantifying this change will help to understand the different flow environments found on the low-pressure turbine over its operational range and how they affect efficiencies of the engine. This paper is a study on how free stream turbulence intensity and Reynolds numbers affect flow separation in modern jet engines.

Introduction

As air passes through a jet engine, the air will transition from a low-pressure, low-energy state to a high-pressure, high-energy state in the combustor just before passing through the turbine. The turbine is a rotary device used to convert energy in a fluid flow into useable work. Once the air has passed through the high-pressure turbine, the low-pressure turbine will then extract additional energy from the flow and convert it into the work needed to drive the fan and low-pressure compressor. Any remaining excess energy after passing through the low-pressure turbine is then converted into the thrust needed to propel the aircraft. Therefore, the less work required to spin the fan and low-pressure compressor, the more thrust is generated for the same amount of fuel. More thrust with less fuel cost results in a more efficient engine.

NASA Glenn Research Center has found that there is a 2% decrease in relative efficiency in an aircraft engine as it travels from sea level at takeoff to the plane's cruise altitude.[1] This decrease in relative efficiency is mainly caused by the occurrence of flow separation in the low-pressure turbine. When flying at high altitudes, flow separation, which causes pressure losses and lowers efficiencies, can be seen on the suction side of the low-pressure turbine blades. Flow separation is when the viscous boundary layer lifts off the surface of a turbine blade, due to an adverse pressure gradient or sharp turns (Figure 1). The top, convex surface of the blade seen in Figure 1 is called the suction surface; the bottom, concave surface is called the pressure surface. This paper is focused on flow separation from the suction surface of the blade.

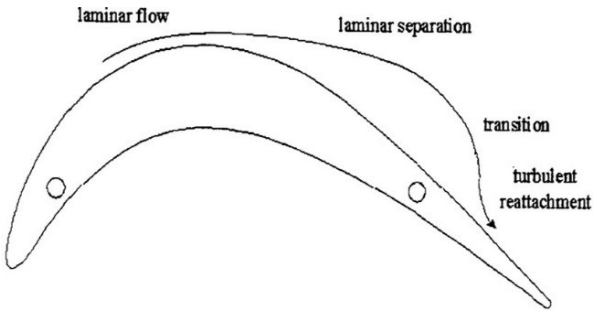

Figure 1. Flow separation on the suction surface of a turbine blade represented by a streamline[2]

The beginning of an adverse pressure gradient is typically located at the maximum thickness of the turbine blade. As the airflow passes the maximum thickness of the blade, the adverse pressure gradient will cause the flow to slow down. This deceleration will cause the boundary layer to separate from the surface of the blade if the airflow enters the adverse pressure gradient with low momentum. This process results in an increase in pressure losses and a decrease in efficiency.

Flow separation has an increased probability of occurring at high altitudes due to a drop in density as the altitude increases. At an altitude of approximately 60,000 feet, the density of air drops to one-tenth of that seen at sea level. This

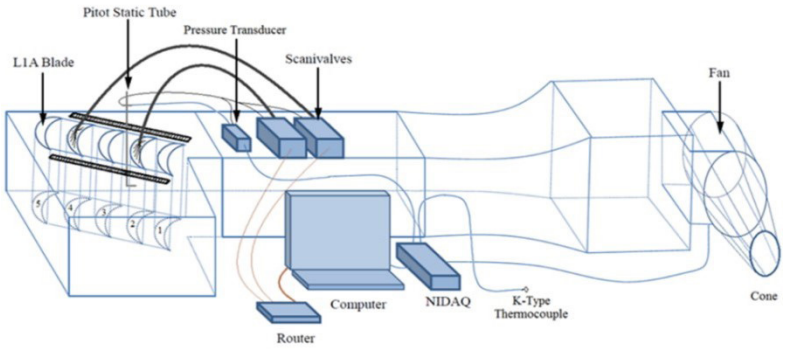

Figure 2. BUC Schematic[10]

low air density combined with a reduced throttle during cruise will typically result in a low Reynolds number between 25,000 and 200,000. A Reynolds number (Equation 1) is the product of the flow velocity, V, the fluid density, ρ, and the characteristic length of the blade, c, all divided by the fluid's dynamic viscosity, μ:

$$\mathrm{Re} = \frac{\rho \mathrm{Vc}}{\mu} = \frac{\text{Inertia Forces}}{\text{Viscous Forces}} \quad (1)$$

The Reynolds number is also described as a ratio comparing the inertial forces in the flow to the viscous forces. A low-Reynolds number flow at high altitudes can be thought of as a low-momentum flow. This is because the density of air has fallen to a reduced value. This lower momentum flow will no longer be able to stay attached as it reaches the adverse pressure gradient and sudden turn of the blade. The flow will therefore separate.

Flow separation in the low-pressure turbine is a significant problem. Many experiments have been conducted in order to better understand the basic characteristics of flow separation at low Reynolds numbers. Volino found that at a high freestream turbulence intensity, the separation bubble was thinner since the separated shear layer was thicker.[3] In later experiments, Volino found that despite having high freestream turbulence intensities present, turbulent shear stress levels may remain low.[4] Also, the location at which the flow transitions from laminar to turbulent moves upstream due to higher Reynolds numbers or higher turbulence intensity. McQuilling *et al.* found that an uncontrolled flow is independent of Reynolds number and turbulence intensity.[5] Bons *et al.* attempted to control flow separation using vortex generating jets in his experiment.[6] The size of the separation bubble was indeed reduced when using vortex generating jets with low duty cycles at about 10%. It was found that the boundary layer remained attached five to six times longer than without the jets. Van Treuren *et al.* studied the effects on flow separation through the use of vortex generators and by varying the freestream turbulence intensity.[7] The results showed that the vortex generators are more effective at reducing flow separation at high Reynolds numbers and high freestream turbulence intensities than they are at low Reynolds numbers and low freestream turbulence intensities. All of these experiments provide information on flow separation and its characteristics to which this study will add. Previous studies have presented research showing that the Reynolds number and free stream turbulence intensity (FSTI) affect not only the size, but also the location of the separation bubble on the suction surface of turbine blades.[8] This paper adds to the research previously conducted and quantifies the effects that varying the Reynolds number and FSTI have on the separation bubble size and location.[9]

Methods and Materials

The BUC is an open circuit cascade wind tunnel designed to simulate low momentum flows, similar to those seen at high altitudes. The BUC consists of several different pieces of equipment used to drive the flow and collect data (Figure 2).

A Cincinnati Blower Fan, model HDBI-160, provides the pressure gradient needed to force air through the BUC. A pitot-static tube connected a Mamac Systems PR-274 pressure transducer which measures and calculates the total, static, and dynamic pressures upstream of the test section.

The DAQ system, used to collect experimental data, consists of three NI DAQ cards (a NI 9211 Thermocouple Input Card, a NI 9205 Analog Input Card, and a NI 9263 Analog Output Card) and a NI compact DAQ 9172 chassis. The thermocouple card measures the temperature of the air using a K-type thermocouple. The input card acquires differential pressure data from the pressure transducer. The output card controls the test section Reynolds number by sending a control signal to the fan. The chassis coordinates data transfer between a NI LabVIEW code and the DAQ cards.

The test section holds 5 L1A profile, model low-pressure turbine blades. Blades 2 and 4 each have 21 static pressure ports on their suction surface and 20 static pressure ports on their pressure surface. Through tubing, the pressure ports are connected to two Scanivalve Digital Sensor Array 3217s (DSAs) which use the pressure ports to measure the static pressure on the surfaces of the blades. Blades one, three, and five were fabricated using a Dimension SST 768 3D printer.

The pressure distribution over the blades is mapped using the coefficient of pressure, C_p which is a dimensionless number that relates the velocity of the flow over the blades to the velocity of the flow upstream of the test section. The coefficient of pressure is the total pressure measured upstream of the

test section, P_T, subtracted by the static pressure measured at each pressure port, $P_{S_{local}}$, all divided by the upstream dynamic pressure (Equation 2).

$$C_p = \frac{P_T - P_{S_{local}}}{\frac{1}{2}\rho V^2} = \frac{P_T - P_{S_{local}}}{P_T - P_S} \quad (2)$$

A constant temperature hotwire anemometer and two traverses were combined to sweep across the BUC and determine the FSTI distribution in the test section. The hotwire consists of an IFA 300 constant temperature anemometer system and a single wire hotwire probe located half an axial chord length upstream of the test section. The hotwire, oriented parallel to the floor of the tunnel, and halfway between the ceiling and the floor, faces directly into the flow from the fan. The hotwire was moved via the upstream traverse in half-inch increments across a 19.5 inch span resulting in 40 points where the FSTI was measured.

Turbulence tests were run at three different Reynolds numbers (60,000, 108,000, and 165,000). At each of these Reynolds numbers, five different turbulence conditions were used: a "clean tunnel" configuration with no turbulence grid and four "dirty tunnel" configurations using turbulence grids of various sizes (0.5 inch, 0.75 inch, 1.0 inch, and 1.5 inches). The construction of the grids was based on a square mesh array of square bars, similar to the grids categorized by Roach.[11]

The pressure variations along the surfaces of the turbine blades are characterized by measuring the C_p at each of the static pressure port locations along blades 2 and 4. C_p tests were also run at the three Reynolds numbers and five different turbulence configurations. The grids used for the C_p tests were the same as those utilized in the turbulence sweep tests. The C_p plots allow the data to be used to visually and quantitatively analyze the flow characteristics seen on the blades at varying Reynolds numbers and FSTIs.

One of the key points in having confidence in the test results was showing flow speed uniformity across the tunnel and proving periodicity. Because blades 1 and 5 are mainly used to provide end wall effects in the test section of the BUC, the pressure distributions on these blades do not need to be known. Blades 2 and 4 are ported, so their pressure distributions are able to be recorded and C_p values plotted. Blade 3, however, is not pressure ported, so the pressure distribution is not known. The concept of periodicity can be used to help validate the testing. Periodicity states that if the velocity between blades 2 and 4 is uniform and the pressure distribution across blade 2 matches the pressure distribution across blade 4, it can be assumed that the same flow characteristics apply to blade 3. This is a very valuable concept for cascade wind tunnels and was a key step in validating the BUC for research.

To prove a periodic condition in the BUC, the tunnel set up was altered before testing to result in a constant velocity distribution across the test section. The velocity sweep test across the tunnel showed a velocity difference between blades 2 and 4 of less than 1%, proving uniform flow, the first step in proving periodicity. This shows a very clean and well configured tunnel.

The next step in proving the BUC produces periodic flow is in matching pressure distributions between blades 2 and 4. C_p plots showed similar pressure distribution between blades 2 and 4 (Figure 3).

The C_p test comparison resulted in a maximum of 1.83% difference between the coefficients of pressure of the two blades. This shows similar pressure distribution and results in meeting the second requirement for proving periodic flow in the BUC.

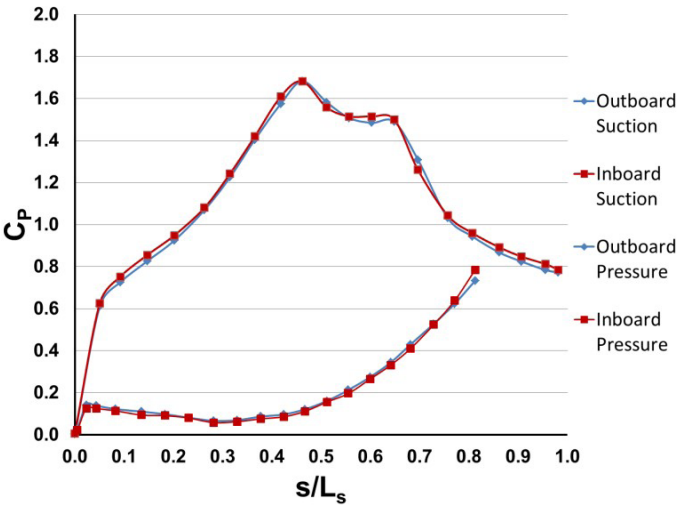

Figure 3. Coefficient of Pressure v. Distance along Suction Surface of L1A Test Blades 2 and 4 at 100,000 Re

Results

Fifteen different tests, each of which consisted of a turbulence sweep test and a C_p test, were performed as a part of this experiment. Each test was run at one of 3 different Reynolds numbers while utilizing one of 5 different turbulence options (the clean tunnel, 0.5 inch grid, 0.75 inch grid, 1.0 inch grid, and the 1.5 inch grid). These different test conditions resulted in Reynolds numbers ranging from 59,233 up to 167,528 and FSTIs ranging from 1.89% up to 19.87%. Each trend seen in the tests was demonstrated for both the clean configuration of the tunnel as well as each of the dirty configurations.

Figure 4 is a graph used to help visualize the results of the turbulence sweep tests when using the 0.5 inch turbulence grid and varying the Reynolds number in the tunnel. The graph shows the FSTI across the test section half an axial chord length upstream of the blades.

The graph contains three curves describing the FSTIs found at the three Reynolds numbers in 0.5 inch increments across the BUC and averaged across blades 2 and 4. Other tests and comparisons were conducted but they showed similar trends to those present in Figure 4.

The comparison in Figure 4 shows the effect that increasing the Reynolds number for a given grid has on the FSTI in the BUC. After conducting turbulence sweep tests under each of the 15 test conditions, two trends were evident. First, as the Reynolds number in the test section increased, the average FSTI increased as well. Figure 4 shows that as the Reynolds number increased from 60,000 to 108,000, the FSTI increased

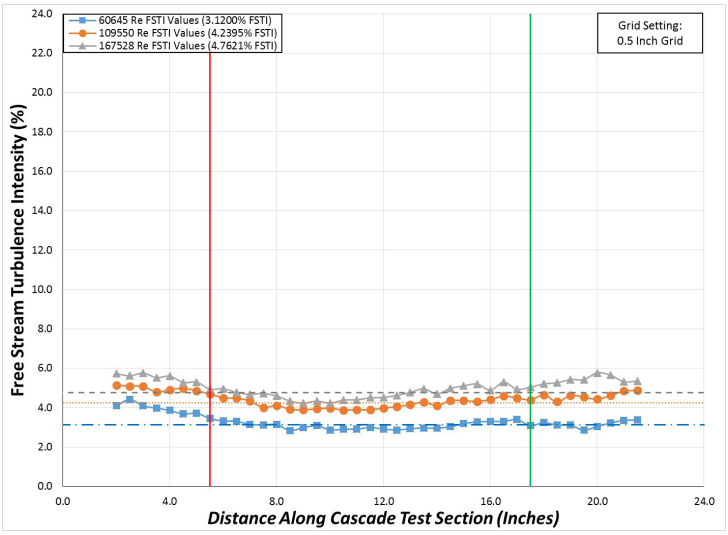

Figure 4. Turbulence Sweep Tests Using the Same Grid while Varying Reynolds Number: *FSTI Graph with 0.5 Inch Grid*

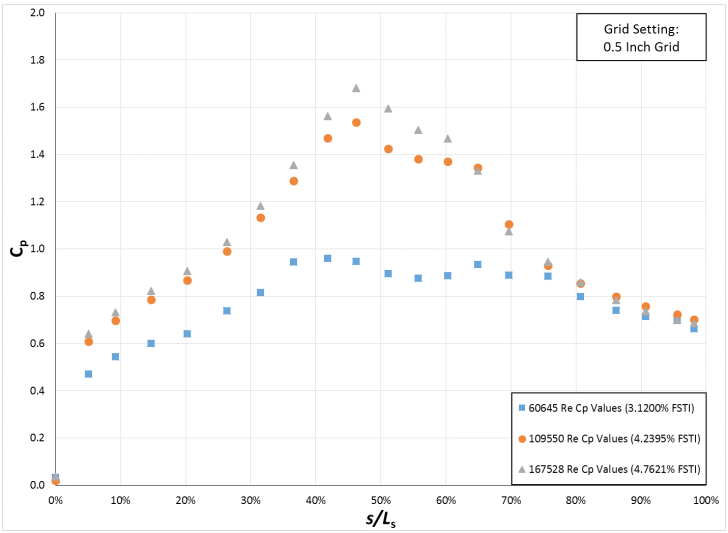

Figure 5. C_P Tests Using the Same Grid while Varying Reynolds Number: *C_p Graph with 0.5 Inch Grid*

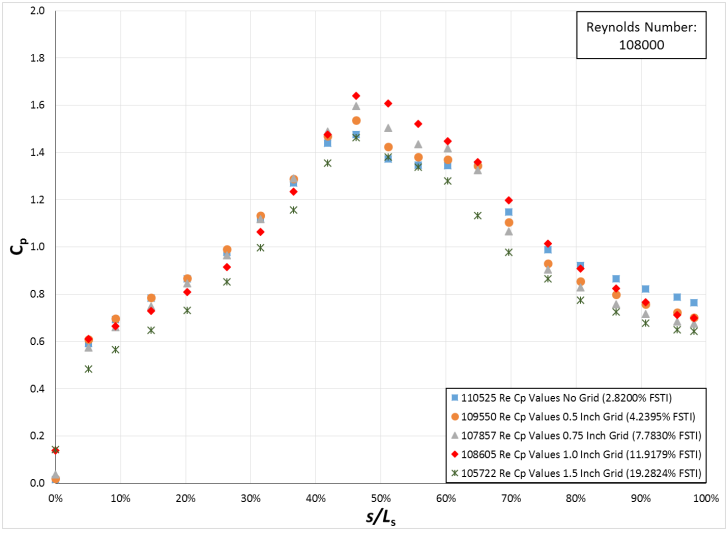

Figure 6. Coefficient of Pressure Tests Using the Same Reynolds Number while Varying Grids: *C_p Graph at 108,000 Re*

by 1.12%, and as the Reynolds number increased from 108,000 to 165,000, the FSTI increased again, but this time by 0.52%. This trend was also shown each time the turbulence grids remained constant and the Reynolds number varied. Second, in each of the five comparisons, FSTI in the tunnel increased faster between 60,000 to 108,000 Re then it did when changing from 108,000 to 165,000 Re (Figure 4).

Figures 5 and 6 consist of graphs that help visualize the results obtained for C_p tests at each of the 15 different conditions. These graphs show how the C_p changes at various points along the suction surfaces of the blades.

Figure 5 shows the C_p tests when using the same turbulence grid in the tunnel but varying the Reynolds number. This graph represents the 0.5 inch grid dirty tunnel configuration. The markers represent the C_ps calculated at the 21 pressure ports along the suction surface of blade 2. The comparison shows the results of the pressure variations along the blades when using the 0.5 inch grid. In Figure 5, the C_p is plotted on the y-axis and the normalized position with respect to the suction surface length, s, is plotted on the x-axis. Other tests and comparisons were conducted but they showed similar trends present in Figure 5.

The graph in Figure 5 shows the effect that altering the Reynolds number has on the coefficients of pressure in the cascade while using the same grid. After conducting C_p tests for each of the 15 test conditions and comparing the results, several trends were shown. First, as the Reynolds number in the test section increased, the separation point moved towards the trailing edge of the blade. Figure 5 shows that as the Reynolds number increased from 60,000 to 108,000, the boundary layer stayed attached longer, and as the Reynolds number increased from 108,000 to 165,000, the separation point moved even farther downstream. This trend was also found each time the turbulence grids remained constant, and the Reynolds number varied. The second trend is that as the Reynolds number changed from 60,000 to 108,000, the reattachment point moved closer to the leading edge of the blade, and when the Reynolds number increased from 108,000 to 165,000, the reattachment point moved even closer to the leading edge. The third trend seen in Figure 5 is that as the Reynolds number changed from 60,000 to 108,000, the separation bubble decreased in size, and when the Reynolds number increased from 108,000 to 165,000, the separation bubble became even smaller.

Figure 6 shows the results of the C_p tests when using different turbulence grids in the tunnel but keeping the Reynolds number constant. The markers represent the C_p calculated at the 21 pressure ports along the suction surface of blade 2. These comparisons show the results of the pressure variations along the blade. The C_p is plotted on the y-axis and the normalized position with respect to the suction surface length, s, is plotted on the x-axis.

The comparisons in Figure 6 analyze the effect that altering the turbulence intensity has on the coefficients of pressure in the BUC at different Reynolds numbers. After conducting the C_p tests for each of the 15 test conditions and comparing the results, three trends were found. First, as the FSTI in the tunnel increased, the separation location moved farther down the suction surface of the blade. Figure 6 shows that as the FSTI increases from 2.82% to 4.24%, the separation location moved farther down the blade, and as the FSTI increases from 4.24% up to 7.78%, the separation location moved even farther downstream. This trend continues until the FSTI jumps from 11.92% to 19.28%. When comparing the C_p graph between these two points, it is shown that the separation location actually moves forward. This is an anomaly not seen in the other tests. It is believed this occurred because of random surging sometimes experienced at high turbulence intensities due to the sudden decrease in cross-sectional area of the 1.5 inch turbulence grid causing unsteady flow. The second trend seen in Figure 6 was that as the FSTI increased, the reattachment point moved closer to the leading edge of the blade. Figure 6 shows that as the FSTI increased from 2.82% to 4.24%, the reattachment location moved closer to the leading edge of the blade and when the FSTI increased again from 4.24% up to 7.78% the reattachment occurred farther from the trailing edge. This trend was seen for every test except when comparing data between the FSTIs of 7.78% and 11.92%. When comparing data between these tests, the reattachment point moved back farther along the blade. This was contrary to the trends viewed in all the other tests. This anomaly is again believed to be due to surging at the high turbulence intensities. The third trend from Figure 6 was that as the FSTI increased, the separation bubble decreased in size.

Discussion

The change in flow characteristics and pressure distributions on L1A low-pressure turbine vanes as FSTIs and Reynolds numbers were varied has been studied. When generating turbulence intensities using square and rectangular bar turbulence grids, eight trends characterizing the effects on surface pressure distributions were found.

The first trend showed that when using the same turbulence grid, an increase in Reynolds number will correlate with an increase in FSTI present in the test section. The second trend showed that the FSTI increased at a faster rate at lower Re values than at higher Re values. The third, fourth, and fifth trends showed that when using the same turbulence grid but varying the Reynolds number, an increase in Reynolds number pushed the separation point closer to the trailing edge of the blade, pulled the reattachment point closer to the leading edge of the blade, and decreased the size of the separation bubble. The sixth, seventh, and eighth trends showed that when using the same Reynolds number but varying the FSTI, an increase in the FSTI pushed the separation point farther along the surface of the blade, pulled the reattachment point closer to the leading edge of the blade, and decreased the overall size of the separation bubble.

Now that the effects of varying turbulence intensities and Reynolds numbers is understood, the next step will be to investigate the heat transfer conditions in the low-pressure turbine. The experiment will be conducted using liquid crystal thermography techniques in order to analyze the heat transfer coefficients in and around the separation bubble. The correlating thermal stresses created by flow separation over the L1A

test blades will also be analyzed. This research topic is critical, because heat transfer in the separation bubble occurs at the same location where turbine blades are the thinnest. This is problematic because the difference in cooling and heating rates at those locations can induce thermal stresses in the blades, causing them to fail prematurely.

Once this research is complete for the L1A, the same experiments conducted in this paper and the heat transfer tests using liquid crystals will be conducted on the L1F blade profile as well.

Nomenclature

Re	Reynolds Number
ρ	Density of a fluid
V	Velocity of a fluid
c	Characteristic Length of the blade
s	Distance along the Suction Surface of the blade
s/L_s	Normalized Distance along the Suction Surface of the blade
μ	Dynamic Viscosity of a fluid
P_T	Total Pressure
P_S	Static Pressure
$P_{S_{local}}$	Local Static Pressure at one point along the blade
C_p	Coefficient of Pressure
FSTI	Free Stream Turbulence Intensity

Acknowledgments

The authors would like to thank Mr. Ashley Orr for his help in machining various parts needed for the research. Thank you also to the Baylor Undergraduate Research in Science and Technology committee for the opportunity to publish in *Scientia*.

References

1. Butler, R. J.; Byerley, A. R.; Van Treuren, K. W.; Baughn, J. W. The Effect of Turbulence Intensity and Length Scale on Low Pressure Turbine Blade Heat Transfer. *Int. J. Heat Fluid Flow.* **2001**, *22*, 123-133.
2. Lake, J. P. Flow Separation Prevention on a Turbine Blade in Cascade at Low Reynolds Number. Report for Air Force Institute of Technology at Wright-Patterson AFB; OH, **1999**.
3. Volino, R. J.; Kartuzona, O.; Ibrahim, M. B. Experimental and Computation Investigations of Separation and Transition on a Highly Loaded Low-Pressure Turbine Airfoil: Part 2 – High Freestream Turbulence Intensity. Presented at ASME International Mechanical Engineering Congress and Exposition, Boston, MA, 2008; Paper IMECE2008-68776.
4. Volino, R. J. Separated Flow Transition Under Simulated Low-Pressure Turbine Airfoil Conditions – Part 1: Mean Flow and Turbulence Statistics. *ASME J. Turbomach*. **2002**, *124*, 645-655.
5. McQuilling, M.; Hollon, B.; Jacob, J. Active Separation Flow Control in a Low Pressure Turbine Blade Cascade Model. AIAA, **2003**; Paper 2003-615.
6. Bons, J. P.; Sondergaard, R.; Rivir, R. B. The Fluid Dynamics of LPT Blade Separation Control Using Pulsed Jets. *ASME J. Turbomach.* **2002**, *124*, 77-85.
7. Van Treuren, K. W.; Simon, T.; von Koller, M.; Byerley, A. R.; Baughn, J. W.; Rivir, R. Measurements in a Turbine Cascade Flow under Ultra Low Reynolds Number Conditions. *ASME J. Turbomach.* **2002**, *124*, 100-106.
8. Pharris, T. M.; Hirst, O. E.; Van Treuren, K. W. Effects of Flow Separation on a Highly Loaded, Low-Pressure Gas Turbine Blade at Low Reynolds Numbers. Presented at ASME International Mechanical Engineering Congress and Exposition, Houston, TX, November 13-19, 2015; Paper IMECE2015-54167.
9. Pharris, T. M; Hirst, O. E.; Van Treuren, K. W. The Generation of Free Stream Turbulence Intensity and its Effects on Flow Separation occurring on a Highly Loaded, Low-Pressure Gas Turbine Blade at Low Reynolds Numbers. ASEE Gulf Southwest Conference, March 6-8, 2016; Paper 145.
10. Becker, J.; Bond, G.; Fox, J.; and Sapp, K. Measuring Flow Separation and Effects of Deposition on a Gas Turbine Blade; Report for Baylor University Mechanical Engineering Laboratory: Waco, TX, 2001.
11. Roach P. E. The Generation of Nearly Isotropic Turbulence by Means of Grids. *Int. J. Heat Fluid Flow*. **1986**, *7*(2), 117-125.

Abstract

Small Molecule Inhibitors of Cruzain as Possible Therapeutics for Chagas' Disease

Hijab Ahmed, Samuel Odutola, Jiangli Song, Mary Lynn Trawick, Ph.D., and Kevin G. Pinney, Ph.D.
Department of Chemistry and Biochemistry, Baylor University, Waco, Texas, USA

Cruzipain, a cysteine protease, plays a major role in the replication and survival of *Trypanosoma cruzi* (*T. cruzi*), the parasitic etiological agent of Chagas' disease, a neglected tropical disease commonly found in Latin America. *T. cruzi* is transmitted into human host cells through ingestion of a blood meal by a triatomine bug. Current medication proves highly toxic in the initial stage and ineffective in the chronic stage, but it is the only available treatment. This warrants further research for other treatments. Since cruzain, the recombinant form of cruzipain, plays an essential role in the development of the parasite, this enzyme is a validated target for developing therapeutics for the disease. Through a collaborative project between the Trawick and Pinney laboratories at Baylor University, a library of small molecule compounds containing the thiosemicarbazone functional group were synthesized and screened as inhibitors of cruzain. Cruzain was obtained via expression in *E. coli* using *T. cruzi* DNA provided by James McKerrow laboratories at the University of San Francisco. The purpose of this study is to validate these compounds as potential inhibitors of cruzain by determining the IC_{50} values against the enzyme. Furthermore, advanced kinetic analyses of these compounds were carried out in order to understand the mechanisms by which these compounds inhibit cruzain. Enzymatic activity of cruzain was monitored using a fluorogenic enzyme assay, which measured the concentration of 7-amino-4-methylcoumarin (AMC) released from Z-FR-AMC, a synthetic substrate. These compounds proved to be effective inhibitors of cruzain in the nanomolar range (20-312 nM) . Progress curves and pre-incubation studies show these compounds as time-dependent inhibitors.

Acknowledgments
I would like to thank Dr. Michelle Nemec of the Molecular Biosciences Center, Dr. Pinney and his lab for synthesizing the compounds.

Resources
1. Chavarria, G.; Horsman, M.; Arispe, W.; Kumar, G.; Chen, S.; Strecker, T.; Trawick, M. Initial evaluation of the antitumour activity of KGP94, a functionalized benzophenone thiosemicarbazone inhibitor of cathepsin L. *Euro. J. Med. Che.* **2012**, *58*, 568-572.
2. 5DPDx – Trypanosomiasis, American. Fact Sheet Centers for Disease Control (CDC).
3. Siles, R.; Chen, S.; Zhou, M.; Pinney, K.; Trawick, M. Design, synthesis, and biochemical evaluation of novel cruzain inhibitors with potential application in the treatment of Chagas' disease. *Bioorg. Med. Chem. Lett.* **2006**, *16*, 4405-4409.

Abstract

Identification of Genetic Signatures in Prostate Cancer using Magnetic Resonance Imaging and Biopsies

Nitheesha Alapati[1], Ellen Hoang[2], and Jessica Maddox[2]
[1]Baylor University, Waco, Texas, USA
[2]Department of Oncology, University of Texas Medical School at Houston, Houston, Texas, USA

A total of 238,590 new cases of prostate cancer in the United States were anticipated in 2013, along with an estimated 28,170 deaths.[1] Prostate cancer deaths are caused by hematogenous metastatic spread and subsequent tumor cell growth in distant sites, primarily bone. The genetic traits that distinguish aggressive from indolent tumors remain unknown. A model that combines multiparametric prostate magnetic resonance imaging (mp-MRI) and next generation sequencing (NGS) from initial biopsy and prostatectomy specimens could potentially distinguish cases of indolent disease not requiring treatment from both those that could be cured with local therapy alone and those of aggressive, potentially lethal disease requiring more rigorous therapeutics.

Unlike biopsies, mp-MRI provides a map of the location, extent, multifocality, volume, index lesion, and aggressiveness of the tumor within the entire prostate. Prostate biopsies underestimate the Gleason score, a measure of prostate cancer severity, in 46% of the cases, and cancer is missed in up to 10%-38% of patients eventually diagnosed with prostate cancer.[2] NGS technologies can detect specific gene signatures in tissue samples. MRI images will be overlaid on biopsy grids to illustrate these signatures associated with areas of varying Gleason scores in biopsies and areas of concern in MRI and to allow more precise, noninvasive tumor staging. Radiogenomics data will illuminate which gene signatures are indicative of tumor indolence versus aggression.

In this study, sixty-six prostate cancer cases were selected from an existing clinical database for a retrospective study. The cases were then organized into these subsets: thirteen with prostatectomy only, seventeen with neoadjuvant chemotherapy followed by prostatectomy, and thirty-six with intact prostate and metastatic disease. These subsets will be analyzed within patients (comparing their normal, low grade tumor, and high grade tumor tissue), within groups, and between groups.

Acknowledgments
I would like to thank Dr. Robert Amato, my Principal Investigator, for his assistance and encouragement throughout the completion of this abstract.

Resources
1. Siegel, R.; Naishadham, D.; Jemal, A. *CA: Cancer J. Clin.* **2013**, *63*(1), 11–30.
2. Shariat, S. F.; Roehrborn, C. G. *Rev. Urol.* **2008**, *10*(4), 262–280.

Abstract

C188-9, A Small-Molecule STAT3 Inhibitor, Effective against Radioresistant Head and Neck Squamous Cell Carcinoma

Oluwatomilona Ifelayo[1], Uddalak Bharadwaj, Ph. D.[2], and David Tweardy, M.D.[2]
[1]Baylor University, Waco, Texas, USA
[2]Division of Internal Medicine, The University of Texas M.D. Anderson Cancer Center, Houston, Texas, USA

The transcription factor Signal Transducer and Activator of Transcription Factor (STAT) 3 is aberrantly activated in many cancers, including Head and Neck Squamous Cell Carcinoma (HNSCC) and is implicated in all major hallmarks of cancer.[1,2] STAT3 also contributes to HNSCC resistance to Ionizing Radiation (IR).[3] A novel drug, C188-9, was recently developed in the Tweardy lab as a STAT3 inhibitor.[4,5] Potent, safe, and orally administered, C188-9 may potentially reduce resistance and improve cure rates for the two-thirds of patients with HNSCC for whom radiotherapy fails.[6,7] One of the first steps, however, to clinical trials is in-vitro tests of drug potency on cancer cells.

Three batches of C188-9 were assessed for potency via an Anchorage-Dependent (AD) MTT based cell growth assay on the radioresistant HNSCC cell line UM-SCC-17B. Though no significant difference existed among the batches, the oldest, which had the lowest half maximal cell growth inhibitory concentration (IC_{50} = 3.0 μM), was used for proceeding tests.

Further testing was conducted to establish an ideal incubation time for optimum cell growth inhibition. C188-9 was tested on two radioresistant (UM-SCC-17B and SQ-20B) and one radiosensitive (SCC-9) cell line using the AD MTT assay with 24, 48, 72, and 96 hour incubation periods. Based on the IC_{50} curves produced, 48 hours was established as the ideal period for subsequent C188-9 AD MTT experiments. 72 hours was used for Anchorage-Independent (AI) assays based on previous experimental protocol.[1] C188-9 was then tested on various radioresistant and radiosensitive cell lines. All cell lines were responsive to the drug (IC_{50} ranging from 2.0 μM to 12.2 μM). Future experiments will include in-vitro assessment of the effect of C188-9 on pSTAT3 activity and expression of IFN/STAT1 signature IR-resistance genes in the IR-resistant HNSCC cell lines (UM-SCC-17B, SCC-35, and Nu-61) and testing whether co-treatment with C188-9 could render these cells IR-sensitive, in both in-vitro and in-vivo testing.

Autophagy is a normal physiological process in the body that deals with destruction of cells in the body. It maintains homeostasis or normal functioning by protein degradation and turnover of the destroyed cell organelles for new cell formation. Tumor cells have been known to upregulate autophagy and this has been linked to IR-resistance. C188-9 was combined with an autophagy inhibitor to determine the type of effect (synergistic or additive) of the two drugs on growth of HNSCC cells via AD and AI MTT assays. These results suggested an additive relationship, but further studies will help precisely model the combined effects.

Acknowledgments
Moses Kasembeli, Ph.D.;
Kris Eckols, Ph.D.;
Prema Robinson, Ph.D.;
and Gayle Slaughter, Ph.D.

Resources

1. Bharadwaj, U.; Eckols, T. K.; Kolosov, M.; Kasembeli, M. M.; Adam, A.; Torres, D.; Zhang, X.; Dobrolecki, L. E.; Wei, W.; Lewis, M. T.; et al. Drug-repositioning screening identified piperlongumine as a direct STAT3 inhibitor with potent activity against breast cancer. *Oncogene.* **2014**, 0.
2. Hanahan, D.; Weinberg, R. A. Hallmarks of cancer: the next generation. Cell. **2011**, *144*, 646-674.
3. Adachi, M.; Cui, C.; Dodge, C. T.; Bhayani, M. K.; Lai, S. Y. Targeting STAT3 inhibits growth and enhances radiosensitivity in head and neck squamous cell carcinoma. *Oral Oncol.* **2012**, *48*, 1220-1226.
4. Redell, M. S.; Ruiz, M. J.; Alonzo T. A.; Gerbing, R. B.; Tweardy, D. J. Stat3 signaling in acute myeloid leukemia: ligand-dependent and -independent activation and induction of apoptosis by a novel small-molecule Stat3 inhibitor. *Blood.* **2011**, *117*, 5701-5709.
5. Redell, M. S.; Ruiz, M. J.; Gerbing, R. B.; Alonzo, T. A.; Lange, B. J.; Tweardy, D. J.; Meshinichi, S.; Children's Oncology Group. FACS analysis of Stat3/5 signaling reveals sensitivity to G-CSF and IL-6 as a significant prognostic factor in pediatric AML: a Children's Oncology Group report. *Blood.* **2013**, *121*, 1083-1093.
6. Harris, A. L. Hypoxia—a key regulatory factor in tumour growth. *Nat. Rev. Cancer.* **2002**, *2*, 38-47.
7. Krstevska, V.; Crvenkova, S. Altered and conventional fractionated radiotherapy in locoregional control and survival of patients with squamous cell carcinoma of the larynx, oropharynx, and hypopharynx. *Croat. Med. J.* **2006**, *47*, 42-52.

Abstract

Experimental and Computational Studies on *Brugia pahangi* Vaccine Antigens

David Le[1], Kevin Shuford, Ph.D.[1], Bin Zhan, M.D., M.S.[2], and Peter Hotez, M.D., Ph.D.[2]
[1]Department of Chemistry and Biochemistry, Baylor University, Waco, Texas, USA
[2]Sabin Vaccine Institute and Texas Children's Hospital Center for Vaccine Development; National School of Tropical Medicine; Baylor College of Medicine; Houston, Texas, USA

A significant public health concern is the control of parasitic nematodes in order to minimize the disease burden of lymphatic filariasis (LF) in endemic regions. The development of a vaccine is a potentially cost-effective approach towards control and elimination of LF.[1] Based on a genome-wide analysis of the developmental stages of the filarial parasite *Brugia pahangi*, molecular targets for interrupting the development of the filarial parasites were identified in Dr. Cheolho Sim's (Baylor University) Lab. Using genetic engineering technology and protein expression systems, these molecular targets can be evaluated as candidates for an innovative transmission blocking vaccine (TBV) against lymphatic filariasis.

These five vaccine antigens were cloned and expressed as recombinant proteins in yeast and bacterial expression platforms. From this, a better purification scheme and a refined expression protocol can be developed to further evaluate expression feasibility. With this preliminary evidence, we believe these proteins are expressible for pilot-scale biomanufacturing for preclinical trials. Further evaluation of the vaccine antigens will prove useful for accelerating and prioritizing them down through the development pipeline.

Bioinformatics screening of the proteinecous vaccine candidates will be used in order to provide a basis for ranking the proteins in priority for antigenic and preclinical study. Using the programs, EpiQuest and EpIC, the primary structure of the proteins will be analyzed in order to identify peptide regions in the sequences that could be epitopes, or antigen recognition sites. Basic Local Alignment Search Tool has identified homologous sequences in each protein sequence. These homologous sequences will enable the use of SWISS-MODEL to develop tertiary and quaternary protein structures using structure-homology modeling algorithms. These theoretical models will then be processed and evaluated for stability through the following computational programs: Anolea, Gromos, DFire, QMEAN6, and Procheck.

Refining the protein structures for greater stability will be done via molecular dynamics simulations using GROMACS. These simulations will then be used for epitope discovery via two computational methods: matrix of local coupling energies and electrostatic desolvation profiles.[2,3] Epitope data from primary and tertiary structures will then be compared to evaluate the antigenicity of the filarial proteins. This computation-based structural vaccinology approach will provide the first protein structures for these biomolecules as well a basis for future experimental endeavors for the development of a TBV. Through these computational biophysical methods and experimental biotechnological techniques, we propose an integrated approach for developing a transmission blocking vaccine that is involves evaluating the feasibility of expression and the antigenicity of the filarial proteins.

Acknowledgments
Dr. Cheolho Sim for his transcriptomic analysis of the *Brugia pahangi* larval development;
Baylor University Collaborative Faculty Research Investment Program Grant

Resources
1. Babayan, S. A.; Allen, J. E.; Taylor, D. W. Future prospects and challenges of vaccines against filariasis. *Parasite Immunol.* **2012**, *34*(5), 243-53.
2. Scarabelli, G.; Morra, G.; Colombo, G. Predicting interaction sites from the energetics of isolated proteins: a new approach to epitope mapping. *Biophys. J.* **2010**, *98*(9), 1966-75.
3. Fiorucci, S.; Zacharias, M. Prediction of protein-protein interaction sites using electrostatic desolvation profiles. *Biophys. J.* **2010**, *98*(9), 1921-30.

Abstract

The Role of Dgcr8 in Post-Natal Kidney Tubule Maintenance

Danae G. Olaso[1], Sachin Hajarnis, Ph.D.[2], Ronak Lakhia, M.D.[2], Matanel Yheskel[2], Vishal Patel, M.D.[2]
[1]Baylor University, Waco, Texas, USA
[2]Department of Internal Medicine, Division of Nephrology, University of Texas Southwestern Medical Center, Dallas, Texas, USA

MicroRNAs (miRNA) are small, non-coding RNAs (about 22 nucleotides) that function in sequence-specific RNA silencing and post-transcriptional regulation of gene expression. MiRNA biogenesis is a multi-step pathway, beginning with the transcription of independent genes to form primary miRNA (pri-miRs) transcripts, which are further processed to ~70 nucleotide long precursor miRNAs (pre-miRNA) by the Drosha-DiGeorge Syndrome Critical Region 8 (Dgcr8) protein complex. The pre-miRNAs are cut by the cytoplasmic protein Dicer to form a ~22 nucleotide long miRNA/*miRNA duplex. Argonaute (Ago) proteins facilitate complementary base pairing between the seed sequence of a mature miRNA and target mRNA on the RNA induced silencing complex (RISC), leading to mRNA degradation or inhibiting translation. MiRNAs play a major role in numerous cellular and developmental processes. The aim of this study was to characterize the role of the miRNA biogenesis enzyme, Dgcr8, in kidney tubule maintenance. Immunofluorescent (IF) staining reveals that Dgcr8 is expressed in the nuclei of tubular cells of the cortical and medullary regions of adult kidneys. Cre/LoxP recombination, a site-specific recombinase technology, was used to knock out the expression of Dgcr8 specifically from the collecting ducts of the mouse kidneys. Western blot analyses confirmed a decrease in Dgcr8 expression in adult mouse kidneys. IF analyses showed that Dgcr8 expression is absent specifically from nuclei of collecting duct cells in knockout mice. Histological analyses at post-natal day 35 (P35) using Hematoxylin and Eosin (H&E) and trichrome staining indicated that the kidneys from Dgcr8 knockout mice developed fibrosis. Renal fibrosis, the excessive accumulation of extracellular matrix in glomerular capillary walls and the interstitial space, is a characteristic feature of all forms of chronic kidney disease. Fibrotic tissue leads to progressive loss of kidney function, while normal tissue maintains the nephron structure and normal physiological function. Thus, because Dgcr8 knockout mice developed renal fibrosis, this indicates that Dgcr8 plays a role in post-natal tubule maintenance in mice kidneys.

Acknowledgments
National Institute of Diabetes and Digestive and Kidney Diseases (NIDDK);
University of Texas Southwestern Medical Center;
and Baylor University

Resources
1. Patel, V.; Hajarnis, S.; Williams, D.; Hunter, R.; Huynh, D.; Igarashi, P. MicroRNAs Regulate Renal Tubule Maturation through Modulation of Pkd1. *J. Am. Soc. Nephrol.* **2012**, *23*(12), 1941–1948
2. Noureddine, L.; Hajarnis, S.; Patel, V. MicroRNAs and Polycystic Kidney Disease. *Drug Discov. Today Dis. Models.* **2013**, *10*(3), e137–e1743

About the Authors

Original Research

Trends of 17β-estradiol Concentrations in the Lake Waco Wetlands - p. 5

Katie Colanero is a sophomore University Scholar from Leawood, Kansas. She is interested in women's health from sociological and biological viewpoints. After graduation, she hopes to attend medical school and one day become an OB/GYN.

Connor Dillon is a sophomore University Scholar from Blue Springs, Missouri. His academic interests include access to health-care and health disparities. In the future, Connor hopes to attend medical school to someday become a practicing physician.

Alexa Larsen is a sophomore Neuroscience major from Chicago, Illinois. She is interested in studying chronic neurological diseases, adolescent medicine, and health disparities. After graduating from Baylor, she hopes to attend medical school to become a pediatrician.

The Effect of Synthetic Sugars on the Photosynthetic Activity of *Chlorella vulgaris* - p. 9

Erin Ahrberg is a sophomore Health Science Studies major from Cushing, Oklahoma. She is interested in studying infectious disease control and prevention. After graduation she hopes to attend medical school and focus her practice in family medicine.

Avery Endsley is a sophomore Chemistry major with a minor in Studio Art from Abilene, Texas. Her research interests include regenerative wound care and healing. Avery hopes to attend medical school and study to become a reconstructive surgeon after graduation.

Daniel Berry is a sophomore Business Fellows major from San Antonio, Texas. His academic interests include chemistry, physiology, literature, Spanish, and epigenetics. Aside from pursing academics, he enjoys playing tennis and spending time with family and friends. Berry aspires to become a physician, incorporating his business background to own a medical practice and serving those around him.

An Empirical Estimation for the Distribution of r^{th} Record Time - p. 12

Jonathan Myers is a senior Applied Mathematics major minoring in Computer Science from Dallas, Texas. He is interested in record values, optimized data analysis, and machine learning. After graduation, he plans to attend graduate school and become a research statistician.

How Varying Reynolds Numbers and Turbulence Intensities Affect Flow Separation on Turbine Blades- p. 15

Tyler Pharris is a senior Mechanical Engineering major from San Antonio, Texas. His research interests include turbulence transition, aircraft design, and propulsion. After graduating from Baylor, he will be interning with SpaceX and then earning his master's degree in Aerospace Engineering.

Olivia Hirst is a senior Mechanical Engineering major from Tomball, Texas. She is interested in turbulent fluid flows and aerospace concepts. After graduation she hopes to continue research in the aerospace industry.

Abstracts

Small Molecule Inhibitors of Cruzain as Possible Therapeutics for Chagas' Disease - p. 21

Hijab Ahmed is a senior Chemistry major from Conroe, Texas. She is interested in identifying small molecule inhibitors of cruzain, an enzyme involved in the pathology of Chagas' disease, a neglected tropical disease. After graduation, she hopes to attend medical school and one day become a physician.

Identification of Genetic Signatures in Prostate Cancer using Magnetic Resonance Imaging and Biopsies - p. 22

Nitheesha Alapati is a senior Business Fellows and Biology major from Dallas, Texas. She is interested in studying small molecule inhibitors of cathepsin L to prevent tumor metastasis. After graduating from Baylor in May, she hopes to attend medical school and become an pediatric oncologist.

C188-9, A Small-Molecule STAT3 Inhibitor, Effective against Radioresistant Head and Neck Squamous Cell Carcinoma - p. 23

Oluwatomilona "Tomi" Ifelayo is a junior Biochemistry major and Biology minor from Richmond, Texas. Her research interests include studying the signal transduction pathways of carcinogenic cell growth and apoptosis. After graduation, she plans to attend medical school, where she will continue to engage in research. She hopes to become a rheumatologist or radiologist.

Experimental and Computational Studies on *Brugia pahangi* Vaccine Antigens - p. 25

David Le is a junior Biochemistry major from Friendswood, TX. He is interested in immunology, systems biology, vaccinology, intellectual history, and theology. After graduating from Baylor, he intends to pursue an M.D.-Ph.D. dual degree.

The Role of Dgcr8 in Post-Natal Kidney Tubule Maintenance - p. 26

Danae Olaso is a senior Biochemistry major and Religion minor from Maui, Hawaii. She is interested in studying the molecular and biochemical basis of kidney disease. After graduation, she hopes to attend medical school and practice as a pediatrician or nephrologist in Hawaii.

Scientia Cover Design

Austin McCrowskie is a junior Graphic Design major from Greenville, Texas. He is interested in photography and visual communication. After graduation, Austin hopes to work for an advertising firm and one day open his own creative studio.

Scientia

For Prospective Authors

Mission

Scientia shall provide a professional platform upon which undergraduates of Baylor University are able to publish personally conducted and outstanding research in the areas of biological sciences, physical sciences, mathematics, and technology.

Accepted Formats

Research Articles presenting original research conducted by current undergraduate level students enrolled at Baylor University. Research articles must include an abstract, introduction, materials and methods, up to six figures or tables, results, and discussion. (Maximum 4500 words, including captions and references.)

Review Articles synthesizing developments of interdisciplinary significance written by current undergraduate level students enrolled at Baylor University. Review articles must include an abstract and an introduction outlining the topic of discussion. (Maximum 6000 words, including captions and references.)

Abstracts proposing research topics currently being investigated by current undergraduate level students enrolled at Baylor University.

For formatting guidelines and submission instructions, please see our website:
http://www.baylor.edu/burst/index.php?id=863108

For Prospective Editors

Are you interested in joining our editorial team? Would you like to help design the next *Scientia*?
Please contact us at burst@baylor.edu.